Three-dimensional Structural Effects of Porous Materials on the Direct-electron-transfer-type Bioelectrocatalysis of Bilirubin Oxidase

Mizue Wanibuchi

2021

Table of Contents

General Introduction

Bilirubin oxidase (BOD) derived from *Myrothecium verrucaria* is a kind of multi-copper enzymes, and is applied to use as an oxygen reduction catalyst. Since BOD functions as a good electrode catalyst in the reduction of O_2 to H_2O, it is frequently used as a biocathode catalyst for biofuel cells.

When there is a direct electron transfer between the enzyme and the electrode, the coupling reaction is referred to as a direct electron transfer (DET) type biocatalytic reaction. The reaction rate constant of the DET-type reaction exponentially decreases with an increase in the distance between the active site in the enzyme and the electrode. Therefore, the distance of the electron transfer pathway and the orientation of the enzyme are important that in the DET type bioelectrocatalysis. In addition, the amount of the enzyme adsorbed on the electrode surface is significant in the DET-type reaction. Various porous materials have been studied for the purpose of improving the characteristics of the DET type reaction because the porous electrode is effective scaffolds for the DET type bioelectocatalysis. The rough surface of the porous electrode is expected to have an advantageous effect on the orientation of the enzyme as compared with the flat electrode. It is thought that the amount of the enzyme absorbed on the electrode dramatically increases. However, there is no quantitative approach on the relationship between the microstructure of porous electrodes and the orientation of the absorbed enzymes. The evaluation guideline using porous materials isn't established yet. In this study, the author used a porous gold electrode made by the anodization method, which makes it easy to control the thickness of the porous structure, and a porous carbon electrode made of three types of carbon materials with different shapes. When a porous carbon electrode was

prepared using a mixture of two types of carbon materials, the suitable properties were achieved in the DET type reaction. The reaction seems to be because the multipoint contact between the BOD molecule and electrode results in higher DET-type bioelectrocatalytic activity. In addition, the mass transport inside the porous structure was simulated based on the method and the effective area of the porous electrode to react with the enzyme and the amount of the effective enzyme were elucidated.

Chapter1

Improved direct electron transfer-type bioelectrocatalysis of bilirubin oxidase using porous gold electrodes

Porous gold (Au) electrodes prepared by anodization of Au electrodes in buffer solutions containing glucose were utilized as scaffolds for direct electron transfer (DET)-type bioelectrocatalysis of bilirubin oxidase (BOD). The three-dimensional porous structure appeared to promote DET-type bioelectrocatalysis of BOD. The current density of DET-type bioelectrocatalysis of BOD increased with the formation of a three-dimensional porous structure at the beginning of anodization; however, it showed saturation characteristics with a further increase in the non-Faradaic current. Moreover, the glucose concentration during anodization affected the activity of DET-type bioelectrocatalysis of BOD. Scanning electron microscopy of the prepared porous Au electrodes showed that the structure of the electrode surface depended on the glucose concentration. Achieving a pore size distribution suitable for substrate transport and enzyme orientation seemed to be dependent on the glucose concentration.

1.1. Introduction

Bioelectrocatalysis is a coupled reaction between a redox enzymatic reaction and an electrode reaction. The direct electron transfer (DET) type of bioelectrocatalysis involves electrons that are transferred directly between an enzyme and an electrode. DET-type bioelectrocatalysis is a promising method for biofuel cells and biosensors because it has a simple construction and is unhindered by the efflux of mediators[1-7]. However, the slow kinetics of electron transfer between electrodes and adsorbed enzymes often limits the practical applications of DET-type bioelectrocatalysis. The rate constant of interfacial electron transfer decreases exponentially with increasing distance between the electrode surface and the redox site of the enzyme[8-10]. Therefore, various modifications of the electrode surface have been proposed to minimize the distance between the electrode and the enzyme[1-7].

It is known that DET-type reactions are enhanced by the use of porous electrodes. One of the reasons is that enlarging the electrode surface area increases the amount of adsorbed enzyme. Additionally, the curvature effects of the porous structure are proposed[2,11-14]. The simulation based on a model with a random orientation of enzymes in a spherical pore suggests that the DET-type activity improves in pores with a size similar to that of the enzyme. When the pore size is similar to the enzyme size, the orientation of the enzymes need not be considered, and the distance between an enzyme redox site and an electrode surface is minimized[15]. On the other hand, large pores are also required for the mass-transport of a substrate from the solution to the adsorbed enzyme. Therefore, the suitable pore size for DET-type bioelectrocatalysis has been investigated[2,16-18]. Various porous media, such as carbon blacks, carbon nanotubes, carbon cryogels, graphenes, and metal nanoparticles, have been investigated in order to improve

the DET-type activity[12-14,19]. However, because the chemical state of the surface functional groups of these materials are not under control and the surface structures of the constructed electrode are not well understood, the curvature effects of these porous media have not yet been clarified. Therefore, it is difficult to establish a suitable surface structure for DET-type bioelectrocatalysis with such materials. Instead, the author has focused on the porous gold (Au) electrode, because its chemical state is relatively stable and its structure can be controlled by selecting appropriate experimental conditions.

In recent years, various methods for constructing porous Au electrodes have been proposed[20]. One of the methods is the utilization of Au nanoparticles, whose size can be controlled by selecting appropriate synthesis conditions[21-24]. However, the 3D-structure of the aggregate is difficult to control precisely, and the capping agents will remain at the surface. Dealloying an alloy of Au and other metals is also a well-established method for preparing nanostructures[25-27]. However, alloying and dealloying processes requires a large environmental load and the preparation of a thin structure without the remaining the other metal is difficult. The anodization of Au in a solution containing a reductant has been explored for use in constructing porous structures[28-31]. This method is simple and easy to control the thickness of the structure. Therefore, the porous Au electrode fabricated by anodization was chosen as the first candidate for the investigation of electrode structures suitable for DET-type bioelectrocatalysis.

Bilirubin oxidase (BOD) derived from *Myrothecium verrucaria* is an enzyme used in many studies on DET-type bioelectrocatalysis[32]. BOD enables DET-type bioelectrocatalytic reduction of O_2 to H_2O[33,34]. BOD has four copper atoms in its two active sites, T1 and T2/3. It is widely accepted that BOD can receive electrons from the electrode at the T1 site and transfer the electrons to the T2/3 site, where O_2 is reduced to

H_2O[34-36]. Because of the high current density and low overpotential of catalytic O_2 reduction, BOD is attracting attention as a catalyst for DET-type biocathodes[37]. It is known that at planar Au electrodes, the DET-type catalytic current of BOD is quite low, while a high catalytic current is obtained at porous Au electrodes[37-40].

Sakai *et al.* have reported the improvement of DET-type bioelectrocatalysis of BOD on porous Au electrodes that were prepared by anodization in oxalic-acid- or glucose-containing solutions[30]. The constructed porous structures were convenient for DET-type catalysis of BOD; however, no detailed information was provided on the relationship between the structure and the DET-type activity. In this work, porous Au electrodes were prepared by anodization at constant potentials in glucose-containing buffer solutions. The effects of anodizing conditions on DET-type bioelectrocatalysis of BOD were investigated. In addition, the structure of the porous Au electrode was observed by scanning electron microscopy.

1.2. Experimental

1.2.1. Materials

BOD (EC 1.3.3.5) from *Myrothecium verrucaria* was purchased from Amano Enzyme Inc. (Japan) and used without further purification. D-(+)-Glucose was obtained from Nacalai Tesque Inc. (Japan). Other chemicals were purchased from Wako Pure Chemical Ind. Ltd. (Japan), and all solutions were prepared with ultra-pure water (> 18.2 MΩ cm^{-1}).

1.2.2. Electrode preparation

Au electrodes with a diameter of 3.0 nm (BAS, Japan) were sequentially

polished with 1 and 0.05 μm alumina slurries followed by sonication and washing with distilled water. The Au electrodes were anodized in a 0.1 M (M = mol dm^{-3}) phosphate buffer (pH 7.0) containing glucose as a reductant at 25 °C. The electrode was rotated at a rotating speed (ω) of 4000 rpm in order to continuously supply glucose to the vicinity of the electrode surface during anodization at a given potential. The charging current of the anodized gold electrode was recorded after repeating the potential cycles until the current response was stable. After washing with the buffer solution (pH 7.0), a 30-μL aliquot of 20 mg mL^{-1} BOD solution dissolved in the buffer solution (pH 7.0) was applied on the electrodes (L = dm^3). The electrodes were left to stand in a water-saturated atmosphere for 1.5 h at 4 °C. The enzyme-modified electrodes were washed with the buffer solution before the electrochemical measurements.

1.2.3. Electrochemical measurements

All electrochemical measurements were conducted on an electrochemical analyzer (ALS 714C, BAS Inc., Japan). Steady-state voltammetric measurements were carried out with rotating disk electrodes (RRDE-2, BAS Inc., Japan) at ω = 4000 rpm and a scan rate (v) of 10 mV s^{-1}. A platinum wire and a Ag|AgCl|sat. KCl electrode were used as the counter and reference electrode, respectively. All potentials in this work are reported with respect to the reference electrode.

1.2.4 Scanning electron microscopy

The surfaces of the anodized porous Au electrodes were observed by a field emission scanning electron microscope (SEM) (SU8000, Hitachi High-Technologies, Japan) at an acceleration voltage of 10.0 kV.

1.3. Results and discussion

1.3.1. Estimation of the electrode surface area

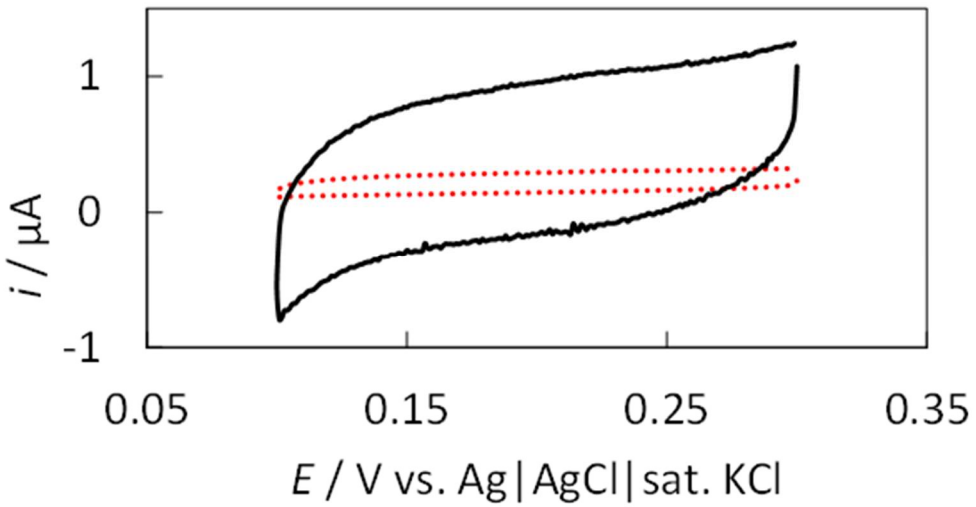

Fig. 1.1 RDCVs of the background charging current at (solid line) the anodized and (dotted line) the planar Au electrodes in 0.1 M phosphate buffer (pH 7.0) under air-saturated conditions at 25 °C, ω = 4000 rpm, and ν = 10 mV s^{-1}. The anodization was performed at 1.7 V and ω = 4000 rpm for 10 min in the presence of 1.0 M glucose.

The Au electrode was anodized at E = 1.7 V and ω = 4000 rpm for 10 min in 1 M glucose solution. After anodization, the electrode surface turned to black. Fig. 1.1 shows the rotating disk cyclic voltammograms (RDCVs) of non-Faradaic charging currents of the planar (dotted line) and anodized Au electrodes (solid line) without BOD. The charging current reflects the electrochemically effective surface areas of the electrodes. The charging current of the anodized electrode was eight times higher than that of the planar electrode. Based on the increase in the charging current and the color change, the anodization of the Au electrode in the glucose solution led to the formation

of nanosized porous structures on the electrode surface. In the following discussion, the ratio of the charging currents of the porous and planar electrodes at 0.16 V was used as to measure the ratio of the electrode surface areas (A/A_{plane}).

1.3.2. DET-type bioelectrocatalysis of BOD on the porous Au electrodes

BOD was adsorbed on the planar and porous Au electrodes. The solid lines in Fig. 1.2 show RDCVs recorded at BOD-adsorbed (a) planar and (b) porous Au electrodes, with A/A_{plane} = 8, under O_2-saturated conditions at pH 7.0, 25 °C, and ω = 4000 rpm. The dotted lines in Fig. 1.2 show the voltammograms recorded under anaerobic conditions. At both electrodes, a catalytic reduction wave was observed. These waves were assigned to DET-type bioelectrocatalytic O_2 reduction by BOD[30,34,37]. At the planar Au electrode, the O_2-reduction current was low, as previously reported[37,40]. On the other hand, at the porous Au electrode, a typical sigmoidal voltammogram was recorded and the catalytic reduction current was 100 times higher than that at the planar electrode. The author hypothesized that the increase in the catalytic current is ascribed to not only the increase in the amount of BOD adsorbed onto the enlarged electrode surface but also the increase in the percentage of productively oriented BOD.

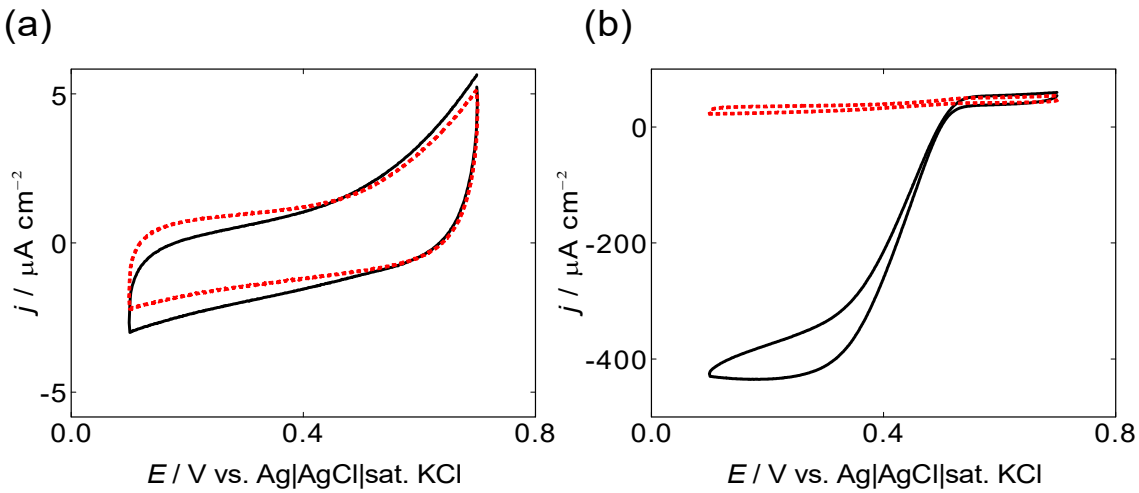

Fig. 1.2 RDCVs of catalytic O_2-reduction at the BOD-adsorbed (a) planar and (b) porous Au electrodes with A/A_{plane} = 8, in 0.1 M phosphate buffer (pH 7.0) at 25 °C, ω = 4000 rpm, and ν = 10 mV s^{-1}. The solid and dotted lines were recorded under O_2-saturated and Ar atmospheres, respectively.

In order to estimate the interfacial-electron-transfer rate constant in the pores, the background-subtracted linear sweep voltammograms of the catalytic O_2 reduction at the BOD-adsorbed Au electrodes were analyzed on the basis of a random orientation model for DET-type bioelectrocatalysis[41,42]. Because the catalytic current density was less than 10% of the saturated-O_2-diffusion-controlled limiting current density (−8.4 mA cm^{-2} at ω = 4000 rpm and 25 °C[43]), a steady-state model without concentration polarization was applied. For the model, the relationship between the steady-state current density (j) and the electrode potentials (E) is given by the following equation:

$$j = \frac{j_{\mathrm{cat}}}{\beta\Delta d(1+\exp\{\Phi\})} \ln\left|\frac{\frac{k_0^{\max}}{k_{\mathrm{c}}}(1+\exp\{\Phi\})+\exp\{\alpha\Phi\}}{\frac{k_0^{\max}}{k_{\mathrm{c}}}\exp(-\beta\Delta d)(1+\exp\{\Phi\})+\exp\{\alpha\Phi\}}\right|, \qquad (1.1)$$

where $\Phi = n'_{\mathrm{E}}F(E - E^{\circ\prime}{}_{\mathrm{E}})/RT$, j_{cat} is the density of the limiting catalytic current, β is the coefficient of long-range electron transfer, Δd is the difference in the distance between the closest and farthest approaches of the redox center of an enzyme that electrochemically communicates with an electrode, n'_{E} is the number of electrons in the rate determining step of interfacial electron transfer (= 1 in this case, as the number of electrons for the T1 site in BOD is 1), F is the Faraday constant, R is the gas constant, T is the absolute temperature, $E^{\circ\prime}{}_{\mathrm{E}}$ is the formal potential of the redox center of the enzyme, $k_0^{\max}$ is the standard rate constant at the distance of the closest approach in the best orientation of the enzyme, k_{c} is the DET-type catalytic constant of the enzyme, and α is the transfer coefficient. Although this model assumes a spherical enzyme adsorbed on a flat electrode, the values of Δd and $k_0^{\max}$ will reflect the curvature effect on the porous electrode. Using j_{cat}, $\beta\Delta d$, $E^{\circ\prime}{}_{\mathrm{E}}$, $k_0^{\max}/k_{\mathrm{c}}$, and α as adjustable parameters, Eq. 1.1 was fitted to the voltammograms using non-linear regression analysis by Gnuplot®.

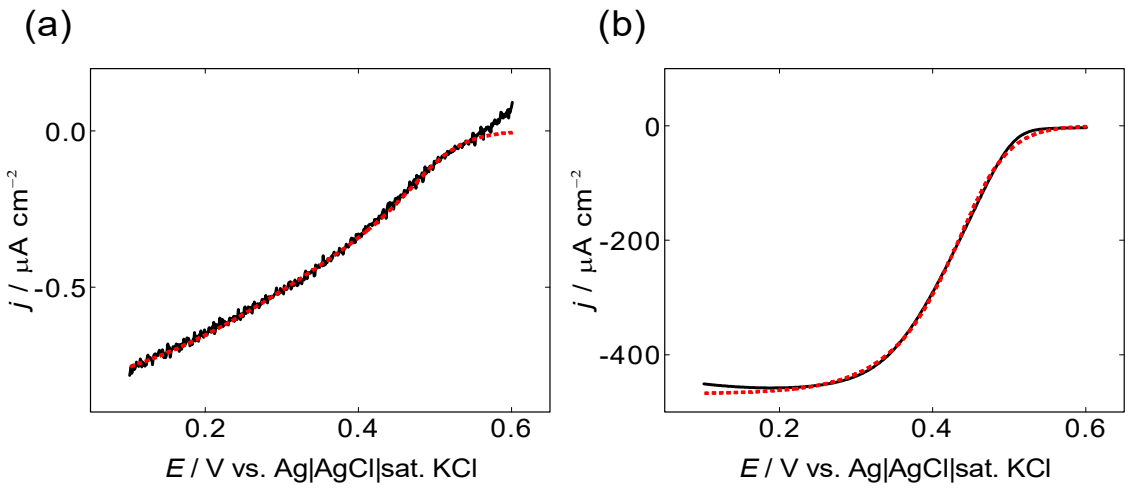

Fig. 1.3 Background-subtracted rotating disk linear sweep voltammograms of catalytic O_2 reduction at the BOD-adsorbed (a) planar and (b) porous Au electrodes in 0.1 M phosphate buffer (pH 7.0) at 25 °C, ω = 4000 rpm, and ν = 10 mV s^{-1} under O_2-saturated conditions (solid line). The dashed lines represent the best-fit curves.

The experimental results were well reproduced by the best-fit curve, as shown by the broken lines in Fig. 1.3. The evaluated values of j_{cat} for planar and porous Au electrodes were –0.86± 0.03 and –466 ± 2 μA cm^{-2}, respectively, which were similar to the values of the limiting current densities in Fig. 1.2. Here, the error range coresponds to the standard error estimated by the fitting procedure. The evaluated values of $E°'_E$ (= 0.47 ± 0.01 for planar Au electrode and 0.45± 0.01 V for porous Au electrode) are similar to the redox potential of the electron accepting site (T1 site) of BOD (= 0.460 V at pH 7.0[44]). Therefore, the direct electrode reduction of T2/3 cluster[45] is negligible at the Au electrodes. The evaluated values of α (0.2±0.1 for planar Au electrode and 0.4±0.1 for porous Au electrode) agrees with the literature value[46,47]. The evaluated values of $\beta\Delta d$

and $k_0^{\max}/k_c$ for porous Au electrode were 2 ± 1 and 2 ± 1, respectively. On the other hand, the evaluated values of $\beta\Delta d$ and $k_0^{\max}/k_c$ for planar Au electrode were 4 ± 2 and 2 ± 2, respectively. Assuming that β for proteins is 1.4 Å^{-1} [48], the Δd values on the planar and porous Au electrodes are 3 ± 1 Å and 1 ± 1 Å, respectively. The small Δd value of the porous Au electrode means that the distribution of the orientation of adsorbed BOD is narrow, that is, the curvature on the porous Au electrode is more suitable for DET-type bioelectrocatalysis of BOD than that on the planar Au electrode. The agreement of estimated values of $k_0^{\max}/k_c$ for the planar and porous Au electrodes demonstrates that the minimum distance between the redox site of BOD and the Au electrode surface is independent of the porous structure. Summarizing the above, the porous Au electrode is more suitable for DET-type bioelectrocatalysis of BOD than the planar Au electrode.

1.3.3. Influence of applied potentials on the preparation of porous Au electrodes

Fig. 1.4 shows the effects of the anodization time on the A/A_{plane} and j at the BOD-adsorbed porous Au electrode. Anodization of the Au electrodes was carried out at (a) 1.6, (b) 1.7, and (c) 1.8 V in 1 M glucose solution. The A/A_{plane} value increased almost linearly with oxidation time. The rate of the increase in the A/A_{plane} value increased with electrode potential (E).

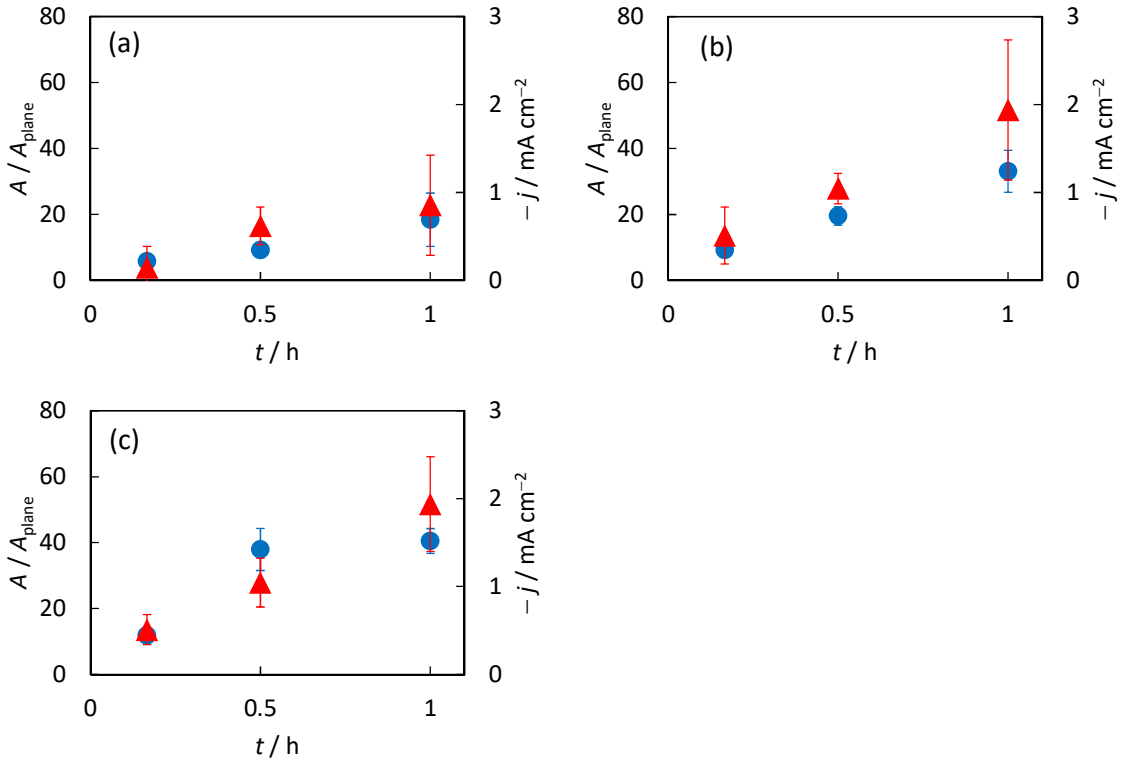

Fig. 1.4 The effects of anodization time on (circle) the relative surface area (A/A_{plane}) estimated from the background current and (triangles) the O_2-reduction current densities (j) at BOD-adsorbed porous Au electrodes at 0.1 V. The Au electrodes were anodized in 1 M glucose solutions at (a) 1.6, (b) 1.7, and (c) 1.8 V. The measurements were conducted in 0.1 M phosphate buffer (pH 7.0) under O_2-saturated conditions at 25 °C, $\omega = 4000$ rpm, and $\nu = 10$ mV s^{-1}.

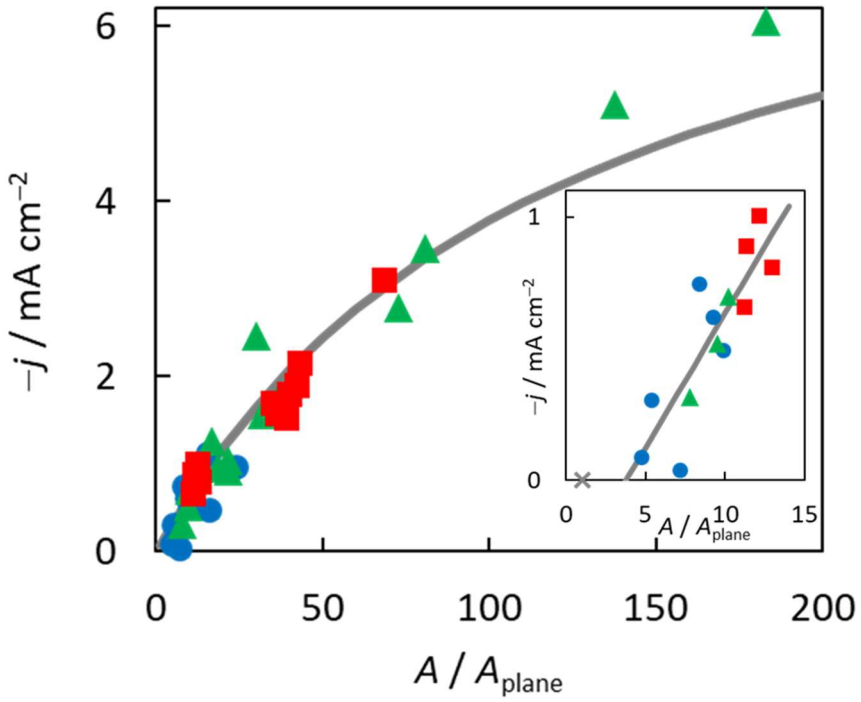

Fig. 1.5 The relation between the catalytic current density (j) at 0.1 V and the relative surface area (A/A_{plane}) at BOD-adsorbed porous Au electrodes anodized at (circle) 1.6, (triangle) 1.7, and (square) 1.8 V. The inset shows an enlargement of the region with small A/A_{plane}.

Fig. 1.5 shows the relationship between the j value at 0.1 V and the A/A_{plane} value. The $|j|$ value increased with an increase in A/A_{plane} and reached a saturated value at increased A/A_{plane}. One of the possible reasons for saturation seems to be an increase in the contribution of the O_2 transport factor to determining j, because the diffusion-limited current density at a rotating disk electrode is -8.4 mA cm^{-2} at $\omega = 4000$ rpm and 25 °C[43]. Another possible reason is that BOD applied on the electrode could not soak into the deep part of the porous structure. The j value was almost independent of the anodizing potentials. This suggests that the j value was simply determined by A/A_{plane}.

The inset in Fig. 1.5 shows a magnified view of the region with small values of A/A_{plane}. In such a small A/A_{plane} region, the relationship between $|j|$ and A/A_{plane} appeared to increase linearly with a negative intercept (or retard increase in $|j|$). The similar retard increase in the DET-type bioelectrocatalysis has been reported for the laccase[24] and oxidation of hydrogen by hydrogenase[23] on the deposited Au nanoparticles on the electrode. In order to clarify the reason, the surfaces of the planar and porous Au electrodes were observed by SEM. Figure 1.6 shows the SEM images of the planar and porous Au electrodes anodized under different conditions. The surface of the planar Au electrode was almost flat (panel (a)), and became rough by the anodization. At A/A_{planar} = 5, the surface of the Au electrode showed step structures identical to a maze of canals; however, the porous structure was not clearly observed (panel (b)). Such step structures seem to be unsuitable for the DET-type reaction of BOD. Most probably, the structure does not provide effective curvature effects in DET-type bioelectrocatalysis of BOD. After deep anodization, clear 3-D porous structures were generated on the Au electrode (panel (c)). The porous structures seem to be constructed from Au nanoparticles with diameter of about 20 nm. The nanoparticles were formed by reduction of the dissolved Au ions by glucose[29]. Because the number of effective pockets in the porous structure increased, the curvature effect seems to be improved for the DET-type reaction.

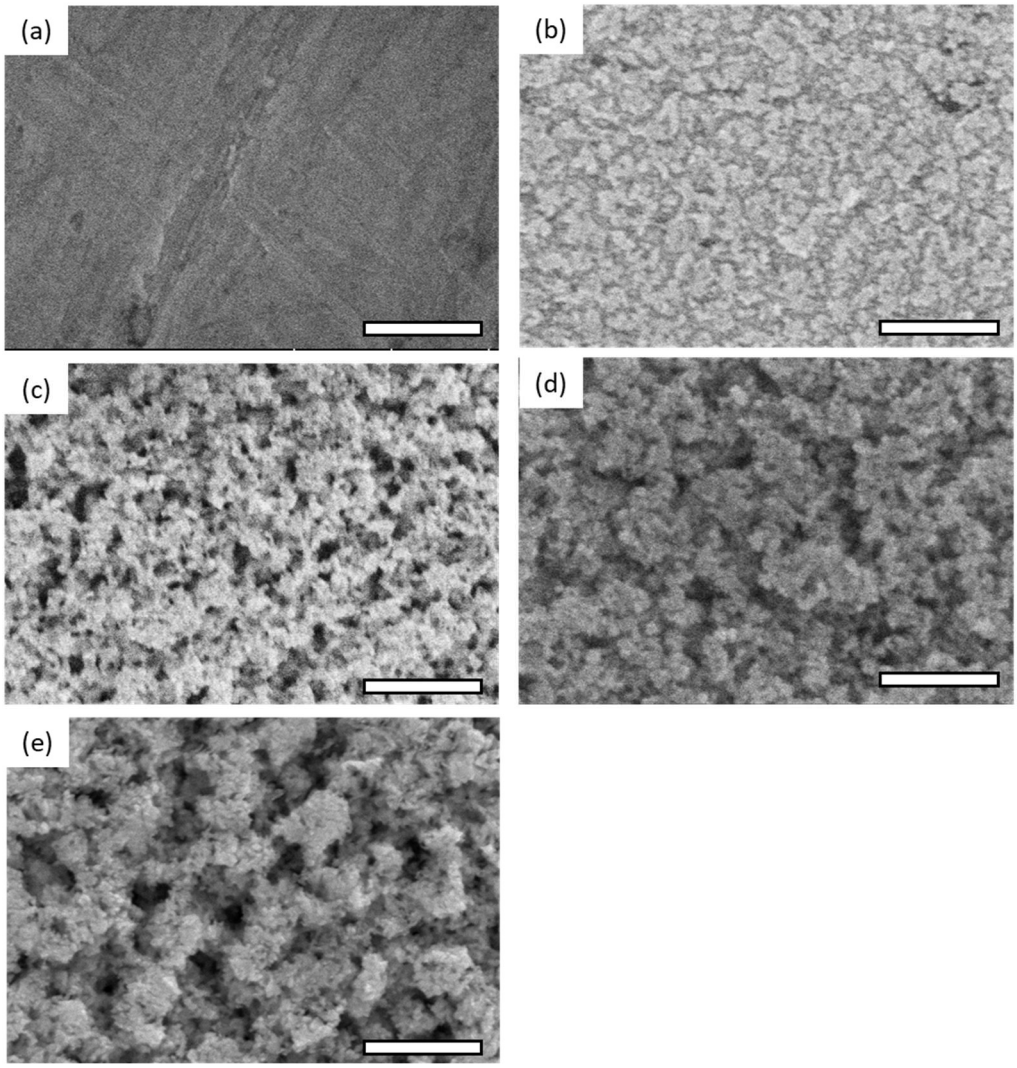

Fig. 1.6 SEM images of the surfaces of the (a) planar and (b-e) anodized Au electrodes. The anodization conditions were: E = 1.7 V; c_{glc} = (b, c) 1 M, (d) 0.5 M, and (e) 0.1 M in 0.1 M phosphate buffer (pH 7); 30 min, ω = 4000 rpm. The resultant A/A_{plane} values were: (a) 1, (b) 5, and (c-e) 20. The scale bars in each panel show 300 nm.

In order to explain the increase in the number of the effective pockets, a simple model of the closed packing spheres on a flat surface was constructed. Fig. 1.7A shows the structures of the packed spheres on a hexagonal lattice at various coverage (θ). The small circles indicate the sites where the number of contacts is more than 3. In this model,

it is assumed that the effective site for the DET-type bioelectrocatalysis has more than 3 contacts. In these small circles, numbers indicate the contact points. O4 and O5 indicate 4 and 5 points contact in the octahedral site, respectively. Assuming that the tetrahedral and octahedral sites are regarded as 4 and 8 three-point contacts, respectively, the total number of contacts (N_c) in each structure were calculated. Fig. 1.7B shows the dependence of calculated N_c in a hexagonal lattice on the surface area of the structure normalized by the flat surface. The linear relationship with negative intercepts in Fig. 1.7B agrees with the experimentally observed relationship shown in the inset in Fig. 1.5. This means that the formation of the 3-D structure is important for expression of the curvature effect. Therefore, the 3-D structure constructed by Au nanoparticles works as the effective scaffold for the DET-type bioelectrocatalysis of BOD.

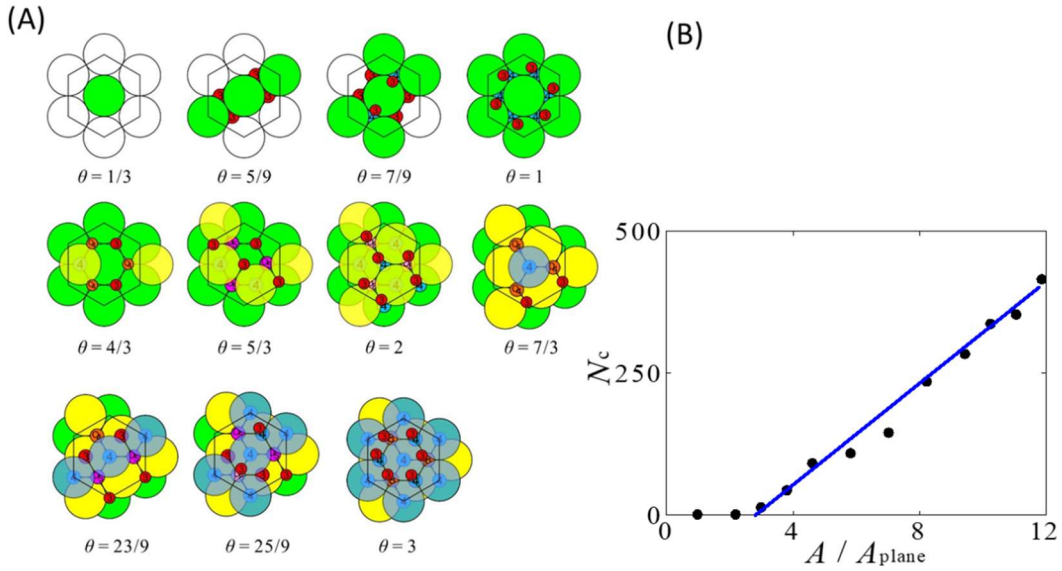

Fig. 1.7 (A) The structure of the closed-packing spheres at various coverage (θ). The small circles indicate the sites where the number of contacts is more than 3. In these small circles, numbers indicate the contact points. O4 and O5 indicate 4 and 5 points contact in the octahedral site, respectively. (B) The increment of the contact numbers with increment of the surface area.

1.3.4. Influence of the glucose concentration on the structure of porous Au electrodes

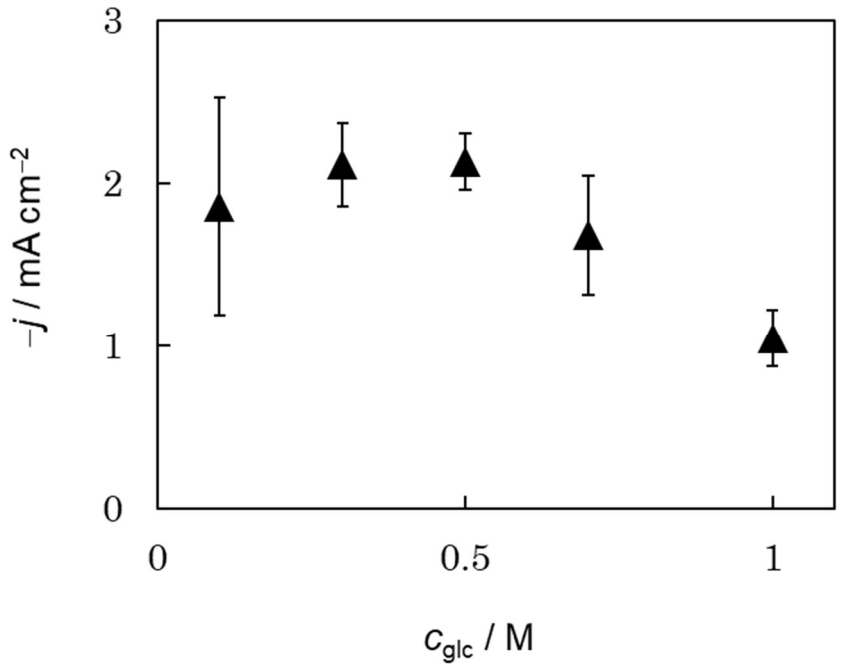

Fig. 1.8 Effects of the glucose concentration (c_{glc}) on the catalytic O_2-reduction current density (j) of BOD-adsorbed porous Au electrodes at 0.1 V, A/A_{plane} = 20, 25 °C, ω = 4000 rpm, and ν = 10 mV s^{-1}.

The author also investigated the relationship between the j values and the glucose concentration (c_{glc}) in the preparation of porous Au electrodes. The porous Au electrodes were prepared by anodization at 1.7 V for 30 min at various c_{glc} values. The A/A_{plane} values were almost independent of c_{glc} and were approximately 20 for all of the electrodes. In contrast, the j value depended on c_{glc}, as shown in Fig. 1.8. At c_{glc} = 0.5 M, the largest $|j|$ was obtained. It can be expected of porous structures to be affected by c_{glc}, because c_{glc} may reflect the reduction power in anodization. In order to clarify this point, the surfaces of several porous Au electrodes were observed by SEM. Panels (c), (d), and

(e) in Fig. 1.6 show the SEM images of the porous Au electrode anodized at c_{glc} = 1 M, 0.5 M, and 0.1 M, respectively. The images clearly indicate that the porous structures depend on c_{glc} in the anodization. At c_{glc} = 1 M, coarsely packed agglomerates and large macropores were observed (panel (c)), most probably due to the fast reduction of dissolved Au ions by glucose without dense packing. In contrast, at c_{glc} = 0.1 M, densely packed agglomerates and large gaps of about 100 nm between the agglomerates (panel (e)) were observed, most probably due to slow reduction of dissolved Au ions. At c_{glc} = 0.5 M, moderately packed agglomerates and relatively small macropores were observed. The moderately packed agglomerates may provide mesopores suitable for the DET-type reaction of BOD due to the curvature effect. However, too densely packed agglomerates seem to be ineffective for holding BOD. The macropores seem to be effective for the mass-transport of O_2 from the bulk phase to the adsorbed enzyme.

1.4. Conclusions

Porous Au electrodes have been prepared under several anodizing conditions, and the effects of the porous structures on the DET-type bioelectrocatalytic performance of BOD have been investigated. The mesoporous structure of the Au surface is convenient for DET-type bioelectrocatalysis of BOD, because the 3-D porous structure on the electrode surface enhances the curvature effects for the adsorbed BOD. The surface area of the porous Au electrode can be enlarged by increasing the anodization time to some extent, though saturation behavior was observed at increased anodization due to the limitations of O_2 transport from the bulk phase and the adsorption of BOD in deep layers. The DET-type bioelectrocatalytic activity of BOD is mainly determined by the surface area of the mesoporous Au electrodes and in part by the glucose concentration during

anodization. The anodizing potential is not an important factor governing the DET-type activity. The SEM observations and the simple closed-packing sphere model have also supported the significance of the mesoporous structures in providing curvature effects for the DET-type reaction. The procedure described here may generate several mesoporous structures suitable for a variety of redox enzymes.

References

1. M. Rasmussen, S. Abdellaoui, and S.D. Minteer, *Biosens. Bioelectron.,* **76**, 91, (2016).
2. I. Mazurenko, A. de Poulpiquet, and E. Lojou, *Curr. Opin. Electrochem.,* 1, (2017).
3. A. dePoulpiquet, D. Ranava, K. Monsalve, M.T. Giudici-Orticoni, and E. Lojou, *ChemElectroChem.* **1,** 1724, (2014).
4. D. Leech, P. Kavanagh, and W. Schuhmann, *Electrochim. Acta*, **84,** 223, (2012).
5. M. J. Moehlenbrock and S.D. Minteer, *Chem. Soc. Rev.*, **37,** 1188, (2008).
6. J.A. Cracknell, K.A. Vincent, and F.A. Armstrong, *Chem. Rev.,* **108,** 2439, (2008).
7. J. Wang, Electrochemical glucose biosensors, *Chem. Rev.*, **108,** 814, (2008).
8. C.C. Moser, J.M. Keske, K. Warncke, R.S. Farid, and P.L. Dutton, *Nature,* **355,** 796, (1992).
9. R.A. Marcus, *Angew. Chem. Int. Ed.* **32,** 1111, (1993).
10. R.A. Marcus and N. Sutin, *BBA Rev. Bioenerg.*, **811,** 265, (1985).
11. A. De Poulpiquet, A. Ciaccafava, and E. Lojou, *Electrochim. Acta*, **126,** 104, (2014).
12. T. Tamaki, *Top. Catal.* **55,** 1162, (2012).
13. A. Walcarius, S.D. Minteer, J. Wang, Y. Lin, and A. Merkoçi, *J. Mater. Chem. B,* **1,** 4878, (2013).
14. D. Wen and A. Eychmüller, *Small*, **12,** 4649, (2016).
15. Y. Sugimoto, Y. Kitazumi, O. Shirai, and K. Kano, *Electrochemistry*, **85,** 82, (2017).
16. L. Bayne, R. V. Ulijn, and P.J. Halling, *Chem. Soc. Rev.*, **42,** 9000, (2013).
17. H. Funabashi, S. Takeuchi, and S. Tsujimura, *Sci. Rep.*, **7,** 1, (2017).

18. S. Hudson, J. Cooney, and E. Magner, *Angew. Chemie Int. Ed.,* **47,** 8582, (2008).

19. C.E. Zhao, P. Gai, R. Song, Y. Chen, J. Zhang, and J.J. Zhu, *Chem. Soc. Rev.*, **46,** 1545, (2017).

20. J. Bhattarai, D. Neupane, B. Nepal, V. Mikhaylov, A. Demchenko, and K. Stine, *Nanomaterials,* **8,** 171, (2018).

21. M. Kizling, M. Dzwonek, A. Wieckowska, and R. Bilewicz, *Curr. Opin. Electrochem.* **12,** 1, (2018).

22. I. Willner, B. Basnar, and B. Willner, *FEBS J.*, **274,** 302, (2007).

23. K. Monsalve, M. Roger, C. Gutierrez-Sanchez, M. Ilbert, S. Nitsche, D. Byrne-Kodjabachian, V. Marchi, and E. Lojou, *Bioelectrochemistry,* **106,** 47, (2015).

24. V. Krikstolaityte, A. Barrantes, A. Ramanavicius, T. Arnebrant, S. Shleev, and T. Ruzgas, *Bioelectrochemistry,* **95,** 1, (2014).

25. U. Salaj-Kosla, S. Pöller, Y. Beyl, M.D. Scanlon, S. Beloshapkin, S. Shleev, W. Schuhmann, and E. Magner, *Electrochem. Commun.* **16,** 92, (2012).

26. H. Qiu, C. Xu, X. Huang, Y. Ding, Y. Qu, and P. Gao, *J. Phys. Chem. C.*, **112,** 14781 (2008).

27. L. Lu, Y. Dong, J. Wang, Q. Li, and X. Wu, *Anal. Methods.,* **7,** 6686, (2015).

28. K. Nishio and H. Masuda, *Bull. Chem. Soc. Jpn.*, **86,** 1144, (2013).

29. Y. Deng, W. Huang, X. Chen, and Z. Li, *Electrochem. Commun.* **10,** 810, (2008).

30. K. Sakai, Y. Kitazumi, O. Shirai, and K. Kano, *Anal. Sci.*, **34,** 1317, (2018).

31. Y. Mie, M. Ikegami, and Y. Komatsu, *Chem. Lett.,* **45,** 640, (2016).

32, S. Tsujimura, T. Nakagawa, K. Kano, and T. Ikeda, *Electrochemistry*, **72,** 437, (2004).

33. N. Mano, *Appl. Microbiol. Biotechnol.* **96,** 301, (2012).

34. N. Mano and L. Edembe, *Biosens. Bioelectron.* **50,** 478, (2013).

35. E.I. Solomon, U.M. Sundaram, and T.E. Machonkin,, *Chem. Rev.*, **96,** 2563, (1996).

36. L. dos Santos, V. Climent, C.F. Blanford, and F.A. Armstrong, *Phys. Chem. Chem. Phys.*, **12,** 13962, (2010).

37. N. Mano and A. De Poulpiquet, *Chem. Rev.* **118,** 2392, (2018).

38. M. Suzukio, K. Murata. N. Nakamura, and H. Ohno, *Electrochemistry*, **80,** 337, (2012).

39. D. Pankratov, R. Sundberg, D.B. Suyatin, J. Sotres, A. Barrantes, T. Ruzgas, I. Maximov, L. Montelius, and S. Shleev, *RSC Adv.* **4,** 38164, (2014).

40. Y. Kamitaka, S. Tsujimura, T. Ikeda, and K. Kano, *Electrochemistry*, **74,** 642, (2006).

41. H.Q. Xia, Y. Kitazumi, O. Shirai, and K. Kano, *J. Electroanal. Chem.*, **763,** 104, (2016).

42. C. Léger, A.K. Jones, S.P.J. Albracht, and F.A. Armstrong, *J. Phys. Chem. B.,* **106,** 13058, (2002).

43. K. So, M. Onizuka, T. Komukai, Y. Kitazumi, O. Shirai, and K. Kano, *Electrochim. Acta.,* **192,** 133, (2016).

44. S. Tsujimura, A. Kuriyama, N. Fujieda, K. Kano, and T. Ikeda, *Anal. Biochem.* **337,** 325, (2005).

45. M. Dagys, A. Laurynėnas, D. Ratautas, J. Kulys, R. Vidžiūnaitė, M. Talaikis, G. Niaura, L. Marcinkevičienė, R. Meškys, and S. Shleev, *Energy Environ. Sci.*, **10,** 498, (2017).

46. Y. Kamitaka, S. Tsujimura, K. Kataoka, T. Sakurai, T. Ikeda, and K. Kano, *J. Electroanal. Chem.* **601,** 119, (2007).

47. J. Lim, N. Cirigliano, J. Wang, and B. Dunn, *Phys. Chem. Chem. Phys.*, **9,** 1809, (2007).

48. C.C. Page, C.C. Moser, X. Chen, P.L. Dutton, *Nature,* **402,** 47, (1999).

Chapter 2

Significance of Nano-Structures of Carbon Materials for Direct-Electron-Transfer-Type Bioelectrocatalysis of Bilirubin Oxidase

Three types of widely used carbon materials were examined as scaffolds for the direct-electron-transfer (DET)-type bioelectrocatalysis of bilirubin oxidase (BOD) as an electrocatalyst for a 4-electron reduction of oxygen (O_2). The carbon materials used were: Ketjen Black EC300J (KB) with a primary particle size (ϕ_p) of ca. 40 nm and a hollow structure, Vulcan XC-72R (Vulcan) with ϕ_p of 37 nm and a filled structure, and high purity graphite SP series (JSP) with ϕ_p of 10 μm and well-developed micropore structures. For the three carbon materials, the rotating disk steady-state limiting catalytic current density of the O_2-reduction ($|j_{c,lim}|$) increased with the non-Faradaic current ($|j_b|$) at small $|j_b|$ values and was saturated at large $|j_b|$ values. The $|j_{c,lim}/j_b|$ ratio in low $|j_b|$ range was in the following order: JSP >> Vulcan > KB. Electrochemical and microscopic data suggested that microporous structures of JSP are highly effective for the DET-type reaction of BOD. Gaps between several primary particles in the KB and Vulcan aggregates play important roles as scaffolds for BOD. The inner surface of partially broken KB particles are electrochemically active to give large $|j_b|$ but not effective as BOD scaffolds.

2.1. Introduction

Mesoporous carbons have been considered as useful electrode materials for direct-electron-transfer (DET)-type bioelectrocatalysis of enzymes[1-5]. The DET-type bioelectrocatalysis is regarded as processes in a series: the mass-transfer of the substrate from the bulk solution to an electrode, the enzymatic reaction, and the interfacial electron transfer between the enzyme and the electrode. The most important process to be considered for the optimization of DET-type bioelectrocatalysis would be the interfacial electron transfer kinetics of large-sized redox enzymes. According to the Marcus theory, the rate constant of the interfacial electron transfer reaction decreases exponentially with an increase in the distance between an electrode surface and the electrode active redox site in an adsorbed enzyme[6-7]. Therefore, the orientation of large-sized enzymes adsorbed on the electrode surface is important to govern the electrode kinetics. In order to minimize the distance between the electrode and the redox site in enzymes, several modifications of the electrode surface have been proposed[1-5,8].

The weight of carbon materials is often used as an important parameter for the optimization of constructions carbon-based porous electrodes for DET-type bioelectrocatalysis. The DET-type bioelectrocatalytic activity of large-sized redox enzymes on the electrode surface strongly depends on the characteristics of the electrode surface[9]. Several researchers have pointed out the importance of the pore size, pore shape, and pore shape distribution important parameters for the adsorption of enzymes[3-4, 9-11].

On the other hand, porous structures of the electrode surface are advantageous for the interfacial electron transfer of redox enzymes by decreasing the distance between enzymes and electrodes since the size of mesoporous structures is comparable to that of enzymes[12-17]. A simple model of a randomly orientated spherical redox enzyme adsorbed

in a spherical pore predicts that a spherical pore with a radius close to that of the enzyme improves the interfacial electron transfer kinetics compared to the flat surface thanks to an increase in the probability of orientations with a short distance in the interfacial electron transfer[13]. This effect is referred to as the curvature effect of mesoporous structures. Under these conditions, the orientation issue of redox enzymes is minimized[13].

Optimization of the size distribution in the mesopores at the electrode surface is also important to improve the DET-type bioelectrocatalysis from the following two standpoints: the mass-transfer of substrates from the solution to the adsorbed enzyme and the penetration of enzyme deep porous structures. Large pores are effective for the transportation of substrates and enzymes[15, 17-18]. Since the penetration of large-sized enzymes into small pores is difficult, the enzymatically effective surface area should be different from the electrochemically active surface area. Therefore, the investigation of the suitablity pore sizes and distributions for DET-type bioelectrocatalysis is an attractive subject in bioelectrochemistry.

Bilirubin oxidase (BOD) from *Myrothecium verrucaria* catalyzes a fast DET-type bioelectrocatalytic reduction of O_2 to H_2O and is the most popular enzyme used as an electrocatalyst for biocathodes for a 4-electron reduction of O_2. BOD has four copper atoms in its two active sites: T1 and T2/3 clusters. It is widely accepted that BOD can receive electrons from the electrode at the T1 site and transfer the electrons to the T2/3 site, where O_2 is reduced to H_2O in 4-electron process[19-20]. Apparent DET-type bioelectrocatalytic activity of BOD is quite small at planar glassy carbon electrodes, while the activity becomes quite high at mesoporous carbon electrodes[5,14-17]. Macropores in carbon materials are highly effective for increasing the amount of adsorbed BOD and mesopores enhance the stability of BOD[15,18]. It is also reported that the electrode

modification with aggregated gold nanoparticles improves the DET-type bioelectrocatalysis of BOD[19-28].

In this work, three types of widely used carbon materials were examined and compared with each other as scaffolds for DET-type bioelectrocatalysis of BOD: Ketjen Black EC300J (KB) with a size of the primary particle (ϕ_p) of 30-40 nm and a hollow structure, Vulcan XC-72R (Vulcan) with ϕ_p of 30-40 nm and a filled structure, and high purity exfoliated graphite J-SP (JSP) with ϕ_p of 10 μm and well-developed micropore structures. In order to characterize the porous electrodes, the author also focused on the electrochemical effective surface area by using a charging current as a measure. The effect of carbon nanostructure on DET-type bioelectrocatalysis was considered on the basis of the electrochemical effective area. In addition, the structure of the carbon material-modified electrodes visualized by scanning electron microscopy and laser microscopy.

2.2. Experimental

2.2.1. Materials

Bilirubin oxidase (BOD) (EC 1.3.3.5) from *Myrothecium verrucaria* was purchased from Amano Enzyme Inc. (Japan) and used without further purification. KB, Vulcan, and JSP were purchased from Lion Co. (Japan), Cabot Corporation (U.S.A.), and Nippon Graphite Co., Ltd. (Japan), respectively. Poly(1,1,2,2-tetrafluoroethylene) fine powder 6-J (PTFE) was purchased from DuPont-Mitsui Fluorochemicals Co., Ltd. (Japan). Unless otherwise specified, all other chemicals were analytical grade and purchased from Wako Pure Chemical Industries, Ltd. (Japan). All solutions were prepared by ion-exchanged water.

2.2.2. Electrode preparation

Glassy carbon (GC) electrodes with a diameter of 3.0 mm (BAS, Japan) were polished with 0.05 μm alumina slurry followed by sonication and washing with ion-exchanged water. Forty mg of each carbon material and 10 mg of PTFE were mixed with 3.5 mL (L = dm^3) of 2-propanol, and the mixture was homogenized with an ultrasonic homogenizer for 10 min. Thereafter, 6.5 mL of ion-exchanged water was added into the slurry, and the mixture was homogenized for 5 min with the ultrasonic homogenizer.

An appropriate amount of the carbon material mixtures was dropped on the surface of the polished GC electrode and dried at room temperature to evaporate the solvent. BOD (0.05 g) was dissolved in 250 μL of a 0.1 M (M = mol dm^{-3}) phosphate buffer of pH 7.0, and 10 μL of the BOD solution was spread on the carbon material-modified GC electrodes. The electrodes were left to stand in a water-saturated atmosphere for 1 h at 4 °C. The enzyme-adsorbed carbon material-modified electrodes were washed with the phosphate buffer solution (pH 7.0) before electrochemical measurements.

2.2.3. Electrochemical measurements

All electrochemical measurements were conducted by an electrochemical analyzer (CompactStat, Ivium Technologies, Netherland). Steady-state voltammetric measurements were carried out with rotating disk electrodes (RDEs) (RDE-1, BAS, Japan) at a rotating speed (ω) of 4000 rpm and a scan rate (v) of 10 mV s^{-1} in an O_2-saturated 0.1 M phosphate buffer solution (pH 7.0). A platinum wire and an Ag|AgCl|sat. KCl electrode were used as the counter and reference electrodes, respectively. All potentials in this work are reported with respect to the reference electrode.

2.2.4. Characterization of the carbon materials

The surfaces of the carbon material-modified electrodes were observed by a field emission scanning electron microscope (SEM) (TM4000, Hitachi High-Technologies Co., Japan) and a laser microscope (Lasertec Co., Japan). SEM measurements were done at an acceleration voltage of 15.0 kV. The specific surface areas of the carbon materials were evaluated from adsorption and desorption isotherms of N_2 at −196 °C recorded by an adsorption apparatus (BELSORP-mini II, BEL Japan Inc.).

2.3. Results and discussion

2.3.1. DET-type bioelectrocatalysis of BOD at various carbon material-modified GC electrodes

Figure 2.1 shows rotating-disk cyclic voltammograms (RDCVs) of O_2 reduction catalyzed in DET-type mode by BOD adsorbed on various amounts of (A) KB-, (B) Vulcan-, and (C) JSP-modified GC electrodes. Clear sigmoidal current-potential curves were observed at all the modified electrodes; BOD worked well as a DET-type bioelectrocatalyst for a 4-electron reduction of O_2 at the carbon material-modified electrodes. In this work, the current density (j) is defined as the current per projective unit area of the electrodes.

The catalytic (Faradaic) and non-Faradaic currents increased with an increase in the weight of the applied carbon materials (W). The KB-modified electrodes provided rather clear limiting values in the catalytic waves, while the Vulcan- and JSP-modified electrodes showed so-called residual slope; the reductive catalytic currents increased almost linearly with a decrease in the electrode potential after the sigmoidal increase. The residual slope is ascribed to the random orientation of the enzyme on the electrodes[13,29].

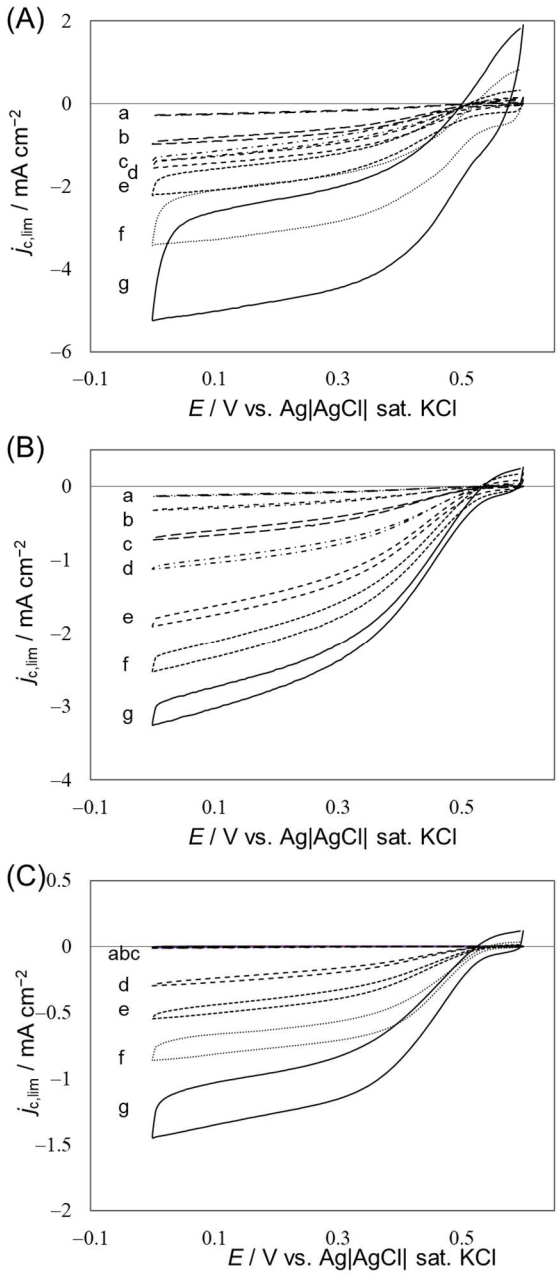

Fig. 2.1. RDCVs of bioelectrocatalytic O_2 reduction at BOD-adsorbed electrodes and KB-modified GC electrodes. The carbon materials used were (A) KB at W = a) 4, b) 8, c) 12, d) 16, e) 24, f) 80, and g) 160 mg, (B) Vulcan at W = a) 4, b) 8, c) 12, d) 16, e) 24, f) 80, and g) 160 mg, and (C) JSP at W = a) 4, b) 12, c) 16, d) 24, e) 80, f) 160, g) 320, and g) 640 mg. The RDCVs were recorded in an O_2-saturated 0.1 M phosphate buffer (pH 7.0) at ω = 4000 rpm, v = 10 mV s^{-1}, and room temperature.

In this work, the background-subtracted catalytic current density measured at 0 V was defined as the limiting one ($j_{c,lim}$), though definitive limiting currents were not obtained in some cases with residual slopes. Considering the mass-transfer and electro-catalytic reaction kinetics, the $j_{c,lim}$ value can be given by a Koutecký-Levich-type equation;

$$\frac{1}{j_{c,lim}} = \frac{1}{j_{dif}} + \frac{1}{j_{cat}} \quad (2.1)$$

where j_{dif} and j_{cat} are, respectively, the limiting current densities controlled by the mass transfer of O_2 at an RDE and by the electro-catalytic reaction kinetics. The j_{dif} value of a 4-electron reduction of O_2 in an O_2-saturated aqueous solution can be estimated by Levich equation to be 8.4 mA cm^{-2} at ω = 4000 rpm and 25 °C[30-31]. The maximum value of the experimentally obtained $j_{c,lim}$ was smaller than the estimated value of j_{dif}. Therefore, the author concluded that under the author's experimental conditions, $j_{c,lim}$ was predominantly determined by j_{cat} given by:

$$j_{cat} = -n_E F k_{cat} \Gamma \quad (2.2)$$

where n_E, F, k_{cat}, and Γ are the number of electrons of the enzyme, the Faraday constant, the catalytic constant (in one catalytic turnover divided by n_E), and the surface concentration of the effective enzyme adsorbed on the electrode, respectively.

The value of W is often used as an important parameter for the optimization of the electrode modification[15,32,34]. Figure 2.2 shows the W value dependence of $j_{c,lim}$. The value of $j_{c,lim}$ increased linearly with W at low W range and showed saturation behavior at increased W range at every carbon material-modified electrode. The saturation behavior obtained at the KB-modified electrodes was similar to that at the Vulcan-modified electrodes, and those $j_{c,lim}$values were much larger than the values at the JSP-modified electrodes. The radii of the primary particles of KB and Vulcan are similar to each other

(about 30 nm), but KB and Vulcan have hollow and filled structures, respectively[33].

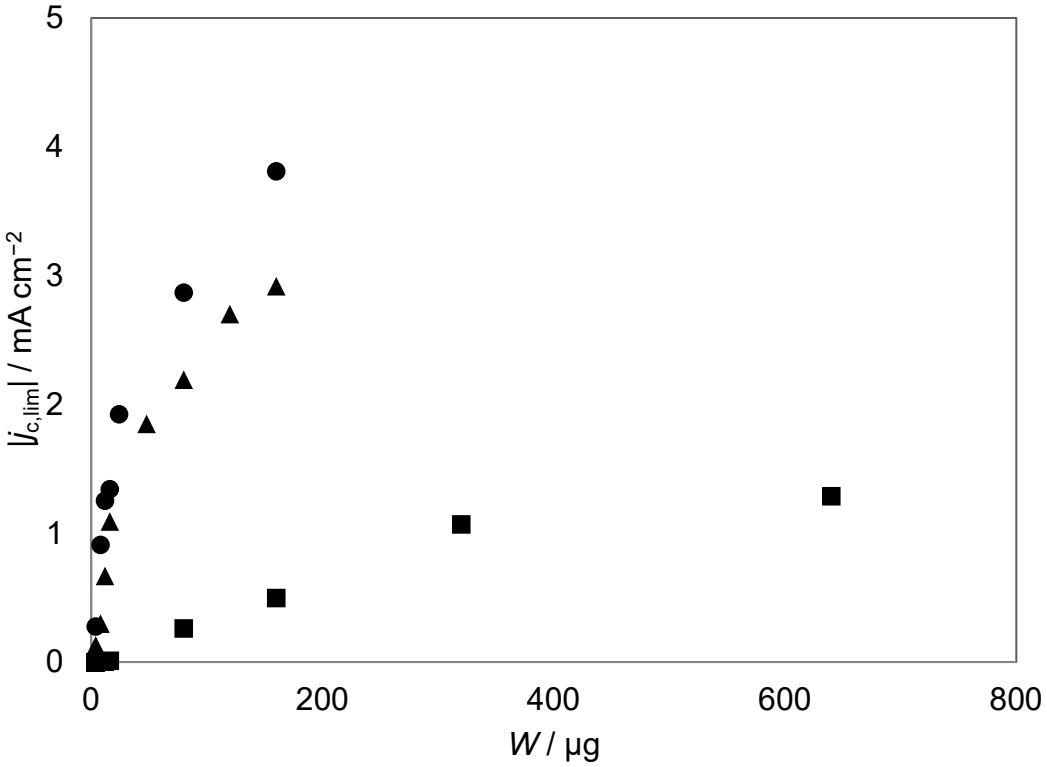

Fig. 2.2. Relationships between the absolute values of the catalytic current density and the weight of applied carbon materials; (●) KB, (▲) Vulcan, and (■) JSP.

Therefore, the specific surface area of KB is much larger than that of Vulcan. Actually, the non-Faradaic currents at the KB-modified electrodes were much larger than that of the Vulcan-modified electrodes (Fig. 2.1). Therefore, Vulcan seems to provide the best characteristics as scaffolds for the DET-type reaction of BOD among them.

3.2. The relationship between $j_{c,lim}$ *and* j_b

Since the effective electrode surface area is an important parameter, in the following the author used the width of the background RDCVs at 0.55 V ($|j_b|$) and at v = 10 mV s^{-1} without BOD (that is, the difference in non-Faradaic (or capacitive) current

densities of the anodic and cathodic scans of RDCVs) as a measure of the electrochemically active surface area. Since the Debye length in the buffer solution is smaller than the primary particle sizes of the carbon materials examined, the value of $|j_b|$ is appropriately considered to correspond to the electrochemically active surface area. Figure 2.3 shows the relationship between $|j_{c,lim}|$ and $|j_b|$ for the three kinds of carbon material-modified electrodes. KB provided large values of $|j_{c,lim}|$ and $|j_b|$. Vulcan provided large values of $|j_{c,lim}|$, while $|j_b|$ values were rather small. JSP gave small values of $|j_{c,lim}|$ and $|j_b|$.

The $|j_{c,lim}|$ values of the three carbon materials increased rapidly with $|j_b|$ at low $|j_b|$ range and tended to be saturated at increased $|j_b|$ range. The estimated slopes at the intersection of the *x*-axes for KB, Vulcan, and JSP are 10, 38, and 133, respectively. As shown in Fig. 2.1, the $|j_b|$ values at the KB-modified electrodes were extremely large compared with those at the Vulcan-modified electrodes, despite that the radii of the primary particles of KB and Vulcan are similar to each other. The primary particle of KB has a hollow structure with a radius of about 10 nm[33]. On the other hand, the primary particle of Vulcan has a filled structure. The primary particles of KB are partially broken and will have holes connected to the inner pore. The electrolyte solution can penetrate into the hole of KB, and then KB gave large $|j_b|$ compared with Vulcan. However, it seems to be difficult for BOD to penetrate the hole of KB. Therefore, the inner surface of the hole of KB would not be utilized as scaffolds for BOD adsorption[34]. These results also show the importance of the outer surface of the primary particles of KB and Vulcan as scaffolds for BOD. Considering very low bioelectrocatalytic activity of BOD at planar GC electrodes[13], the outer surface of the primary particle with a radius of ca. 30 nm does not seem to be suitable scaffolds for BOD.

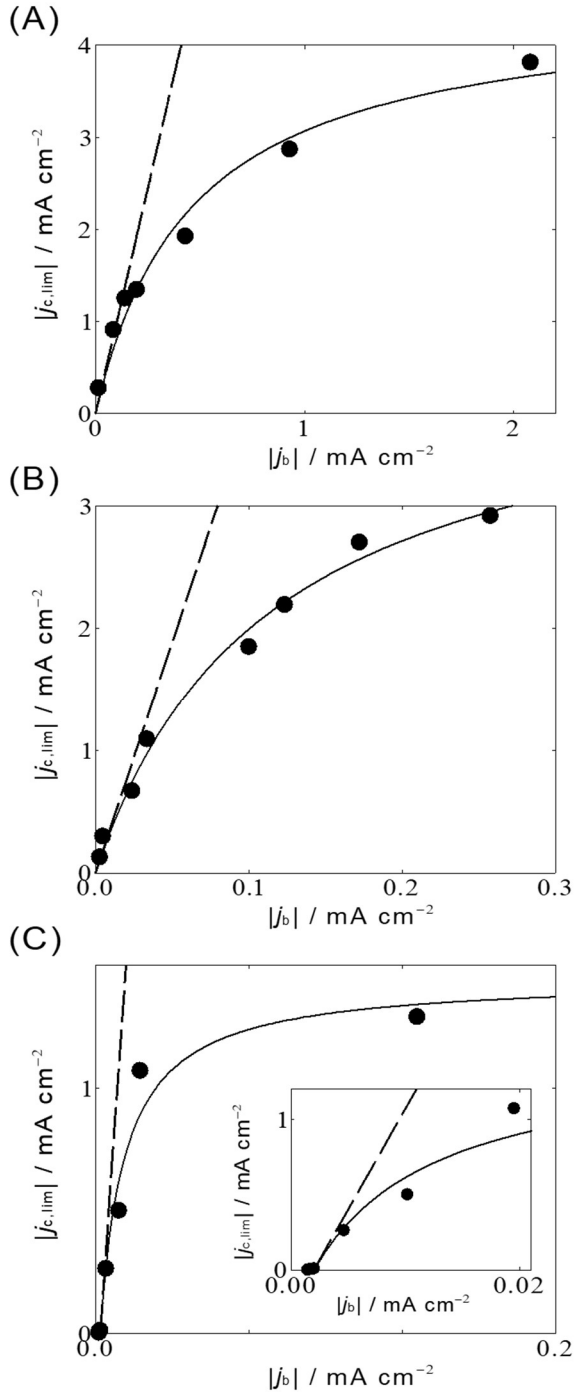

Fig. 2.3. The relation between the absolute value of the catalytic current density and the background current density at the three-carbon material-modified electrodes. (A) KB, (B) Vulcan, and (C) JSP. The inset in panel C shows a magnified view around the origin. Broken lines indicate the slopes at the intersection at the *x*-axes.

Therefore, the aggregation of KB and Vulcan seems to be essential for DET-type communication of BOD with the carbon materials as in the case of gold nanoparticles[35]. The gaps among several primary particles in the aggregate seem to play important roles as scaffolds for BOD thanks to curvature effects of the gap-type mesoporous structures.

On the other hand, the situation for JSP is completely different. The size of the primary particle of JSP is very large (10 μm) compared to BOD (5 nm). Therefore, the size of the gap among the particles in the aggregate of JSP is too large for the DET-type communication of BOD. However, the slope of the $|j_{c,lim}|-|j_b|$ curve of JSP at low $|j_b|$ is the largest among the carbon materials examined. JSP is characterized to develop relatively higher degrees of microporous structures (Fig. 2.8). On the other hand, the increased electric field at the edge of microstructures is considered to enhance the interfacial electron transfer kinetics[36-37]. Therefore, the author can conclude that the microporous structures at the surface of JSP are very effective for the DET-type reaction of BOD.

However, the $|j_{c,lim}|$ values of JSP at increased $|j_b|$ region was much lower than those of KB and Vulcan. The aggregate of JSP with a large ϕ_p does not seem to be suitable for the DET reaction of BOD. Most probably, the penetration of BOD into a stacked JSP layer was difficult. Some hindrances in the mass transfer of O_2 into a stacked JSP layer may also occur.

2.3.3. Microscopic observation of aggregated carbon materials

In the case of gold nanoparticles, initial straight relations in $|j_{c,lim}|-|j_b|$ curves often give negative intercepts[19-28, 37]. This is also ascribed to the significant contribution of gaps constructed among gold nanoparticles; such gaps are not formed at very low surface coverage due to the rather homogeneous distribution of gold nanoparticles[35]. In the case of JSP, the negative intercept of the initial straight region is observed. However, in the cases of KB and Vulcan, the straight lines in Fig. 2.3 go through the origin. This seems to be ascribed to the inhomogeneous distribution of the carbon particles and formation of aggregations on the electrode surface even at low surface coverages of KB and Vulcan. In order to justify the prediction, microscopic observation of the carbon materials on the electrode surfaces was carried out.

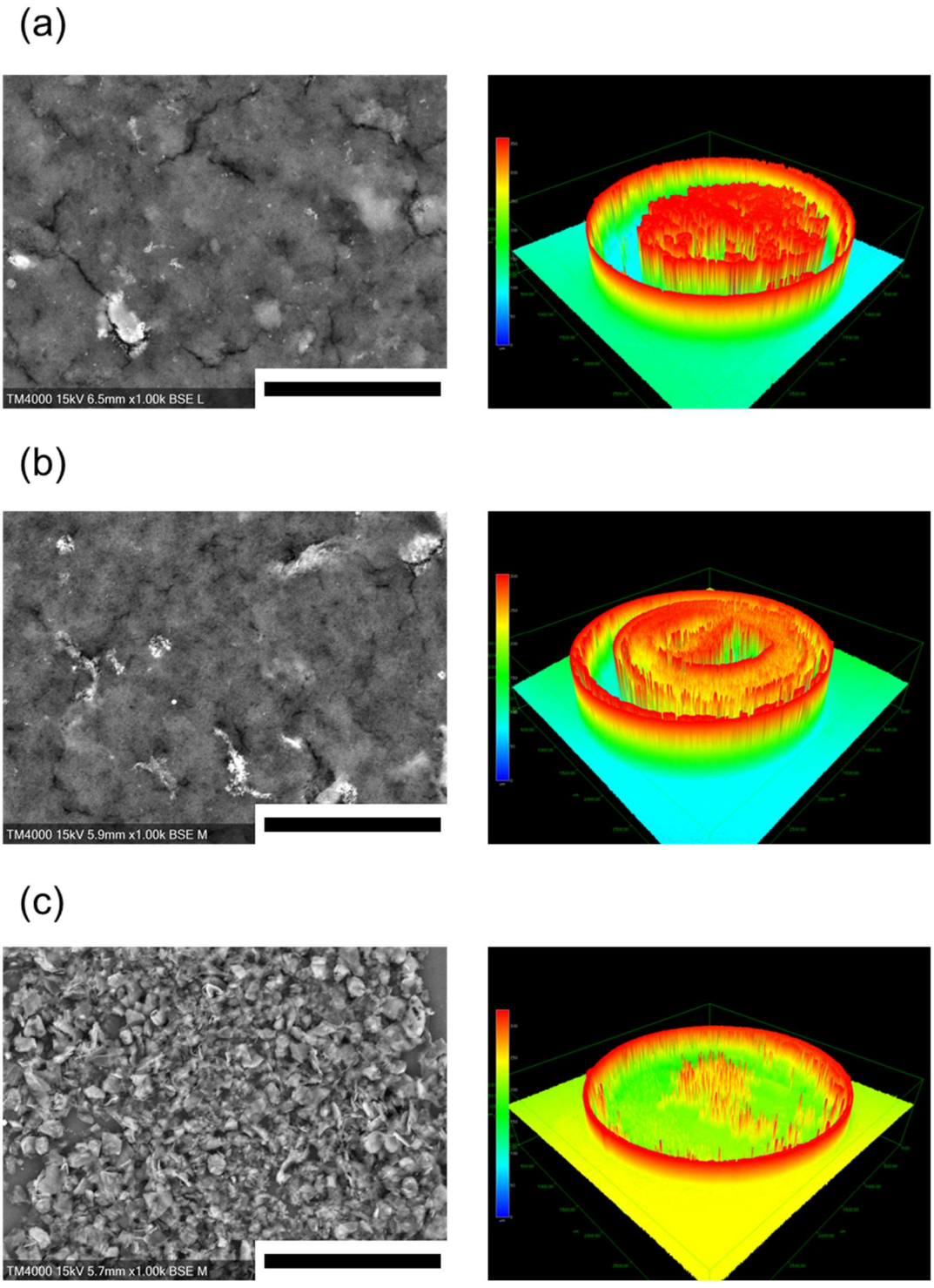

Fig. 2.4. SEM (left) and laser microscopy images (right) of the carbon material-modified GC electrode surfaces of (a) KB 4 μg, (b) Vulcan 4 μg, and (c) JSP 4 μg. The scale bars in SEM and laser microscopic images indicate 50 μm, and 1 mm, respectively.

Figure 2.4 shows SEM and laser microscopy images of the three kinds of the carbon materials examined on the GC electrodes at very low *W* values in the range of the straight relation between $|j_{c,lim}|$ and *W* (Fig. 2.2). The distribution patterns of KB and Vulcan were similar to each other., while those of JSP were somewhat different from those of KB and Vulcan. The difference in the distribution patterns seems to be ascribed to the difference in the radii of the primary particles of the carbon materials. In any events, the microscopic observation well supported the author's prediction; KB and Vulcan were not uniformly dispersed on the GC surface and aggregates were formed when low amounts of the carbon materials were dispersed. The laser microscopy of the JSP modified electrode shows the distribution of JSP at the GC surface is relatively homogeneous. The aggregation seems to occur due to the hydrophobic interaction of the carbon particles in the drying process. Therefore, gap-type mesoporous structures effective for the DET-reaction of BOD can be formed among the carbon particles even at low surface coverages of the carbon materials. This seems to be the reason that the $|j_{c,lim}|-|j_b|$ curves go through the origin. The situation is different from that of gold nanoparticles[19-28,37].

When the amounts of the carbon materials were increased, the aggregates macroscopically appeared to homogeneously cover the electrode surface (Figs. 2.5-7.).

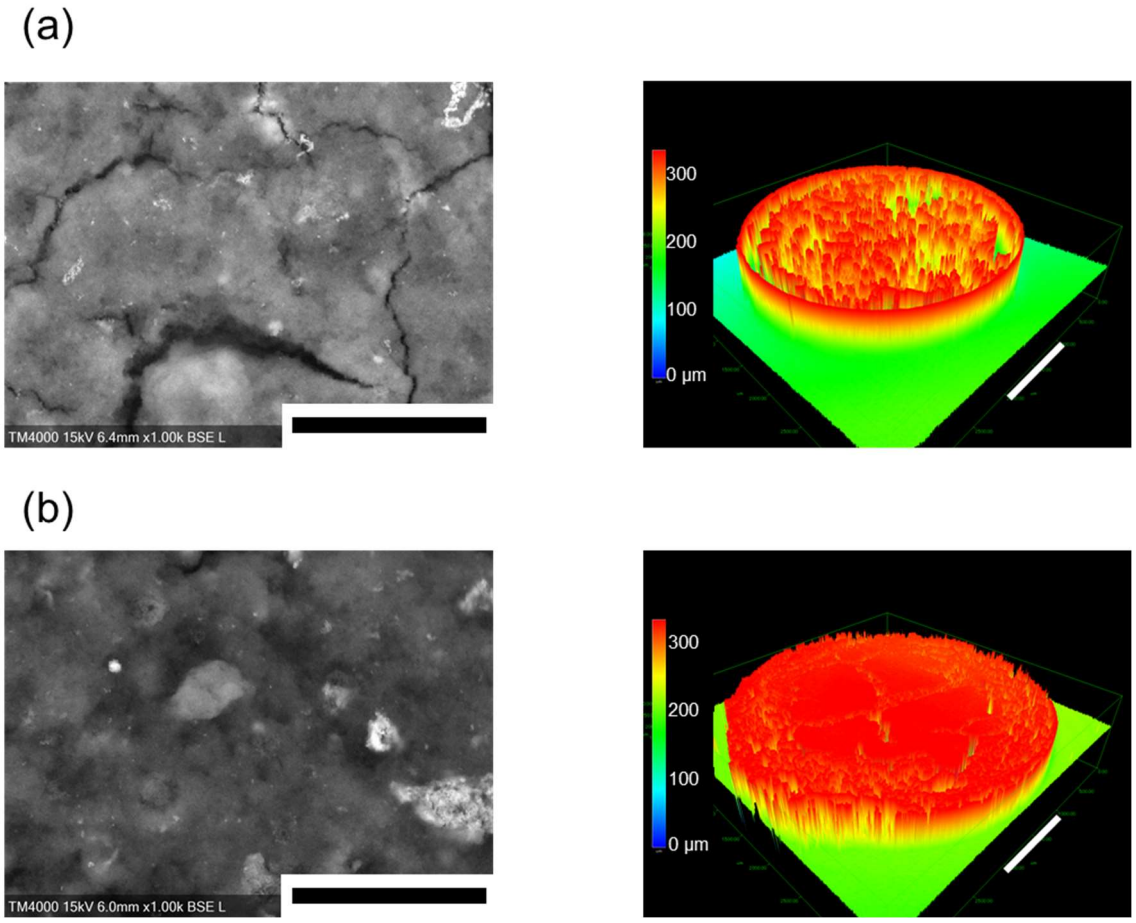

Fig. 2.5. SEM (left) and laser microscopy images (right) of the KB-modified GC electrode surfaces at W = (a) 16 μg and (b) 160 μg. The scale bars in SEM and laser microscopic images indicate 50 μm, and 1 mm, respectively.

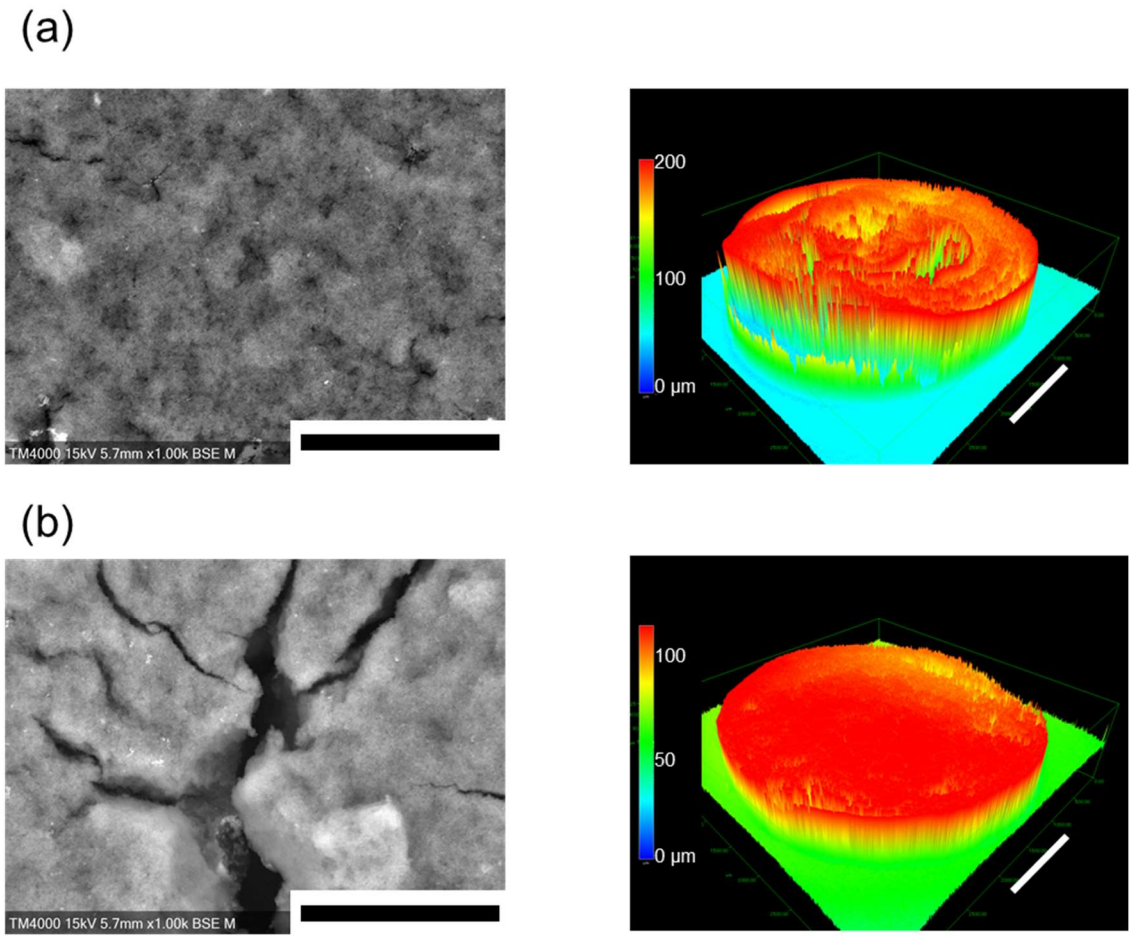

Fig. 2.6. SEM (left) and laser microscopy images (right) of the Vulcan-modified GC electrode surfaces at W = (a) 16 μg and (b) 120 μg. The scale bars in SEM and laser microscopic images indicate 50 μm, and 1 mm, respectively.

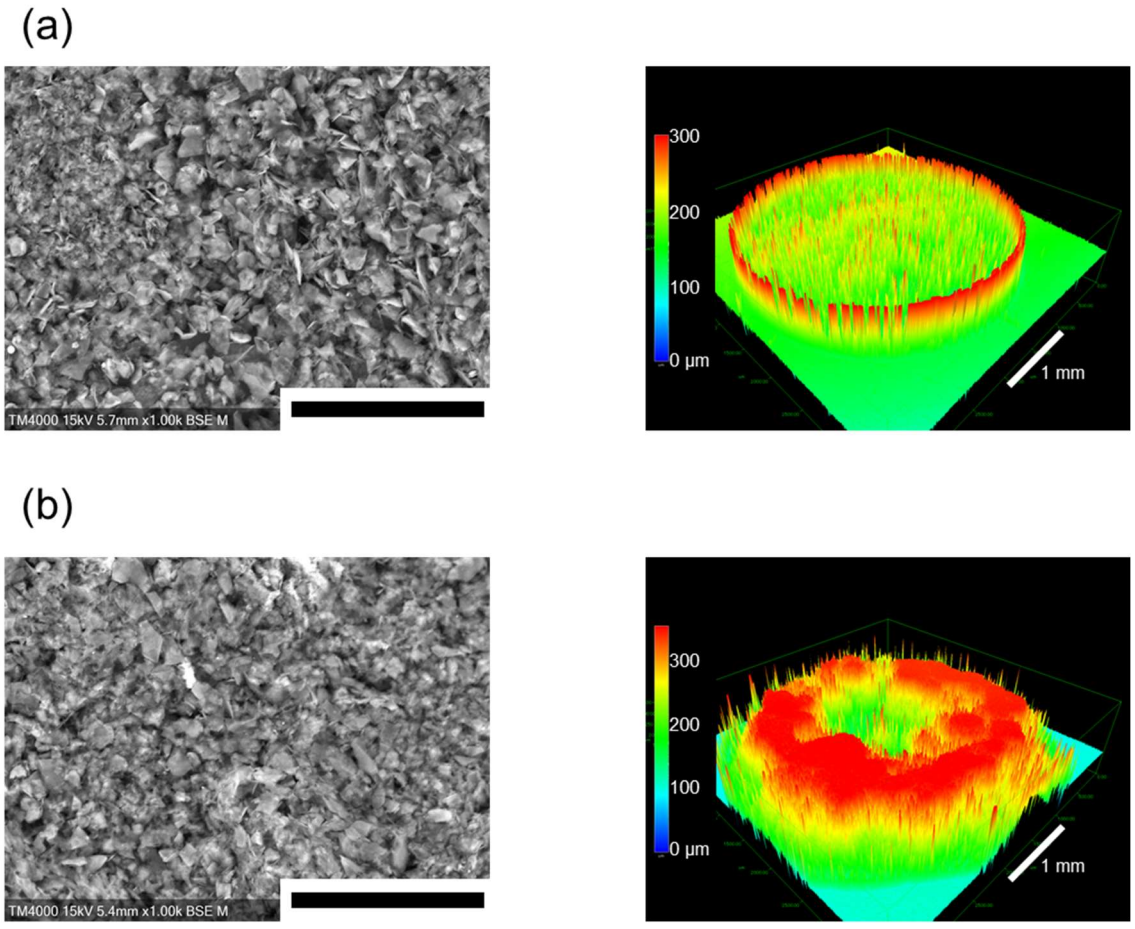

Fig. 2.7. SEM (left) and laser microscopy images (right) of the JSP-modified GC electrode surfaces at W = (a) 16 μg and (b) 640 μg. The scale bars in SEM and laser microscopic images indicate 50 μm, and 1 mm, respectively.

However, the surface of the aggregates of KB and Vulcan had deep cracks. These cracks are also formed during the drying process. Such large cracks themselves do not seem to play important roles in DET-type reactions of BOD, as judged from the results in Fig. 2.2[38].

In the case of JSP, the particle size is comparable to the thickness of the diffusion layer at the RDE at 4000 rpm ($nFDc$ / 8.4 mA cm^{-2} = 10 μm). The number of paths of the substrate transfer from the bulk solution into the aggregates of JSP seems to

be very limited and the path length would be rather long compared with the diffusion layer thickness. Since the structure of densely packed JSP showed disadvantages for the substrate transfer, the saturated value of $|j_{c,lim}|-|j_b|$ for JSP is smaller than that for KB or Vulcan. One of the advantages of JSP maybe that cracks were not observed at increased *W*. This property may be utilized as a base of scaffold for enzyme adsorption.

Since the electrolyte solution may be difficult to penetrate (hydrophobic) microporous structures of carbon materials, the electrochemically effective area does not necessarily coincide with the specific surface area determined, for example, by gas adsorption, as shown in Fig. 2.8. The estimated BET surface area was 720, 230, and 11 $m^2\ g^{-1}$ for KB, Vulcan, and JSP, respectively. The values of $|j_b|$ linearly increased with increasing *W* on the electrode surface, as shown in Fig. 2.9. The slopes for KB, Vulcan, and JSP are 0.015 ± 0.002, 0.0022 ± 0.002, and 0.00004 ± 0.00001 mA cm^{-2} μg^{-1}, respectively. The ratio of the BET surface area and the slope for KB agrees with that for Vulcan. On the other hand, as mentioned above, these ratios disagree with that for JSP, since the penetration of the electrolyte into micropore is difficult. The $|j_{c,lim}|-|j_b|$ curves show characteristics of the saturation, since the penetration of the enzyme into mesopores in the stacked JSP is also difficult. In addition, the mass transfer of O_2 seems to be inhibited in the densely packed layer of JSP, though JSP particles provide a suitable scaffold for the DET-type reaction of BOD at low surface coverages.

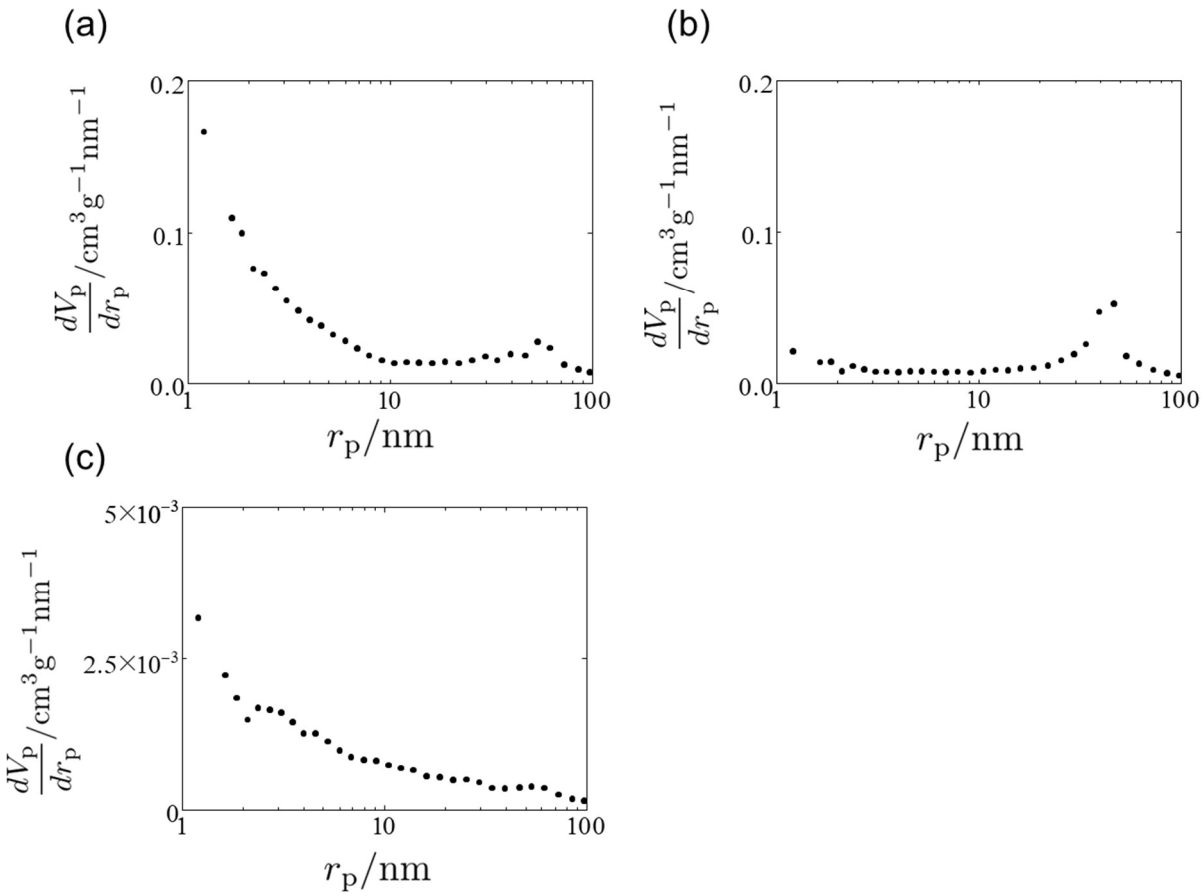

Fig. 2.8. Pore size distribution of (a) KB, (b) Vulcan, and (c) JSC estimated by the Dollimore-Heal method.

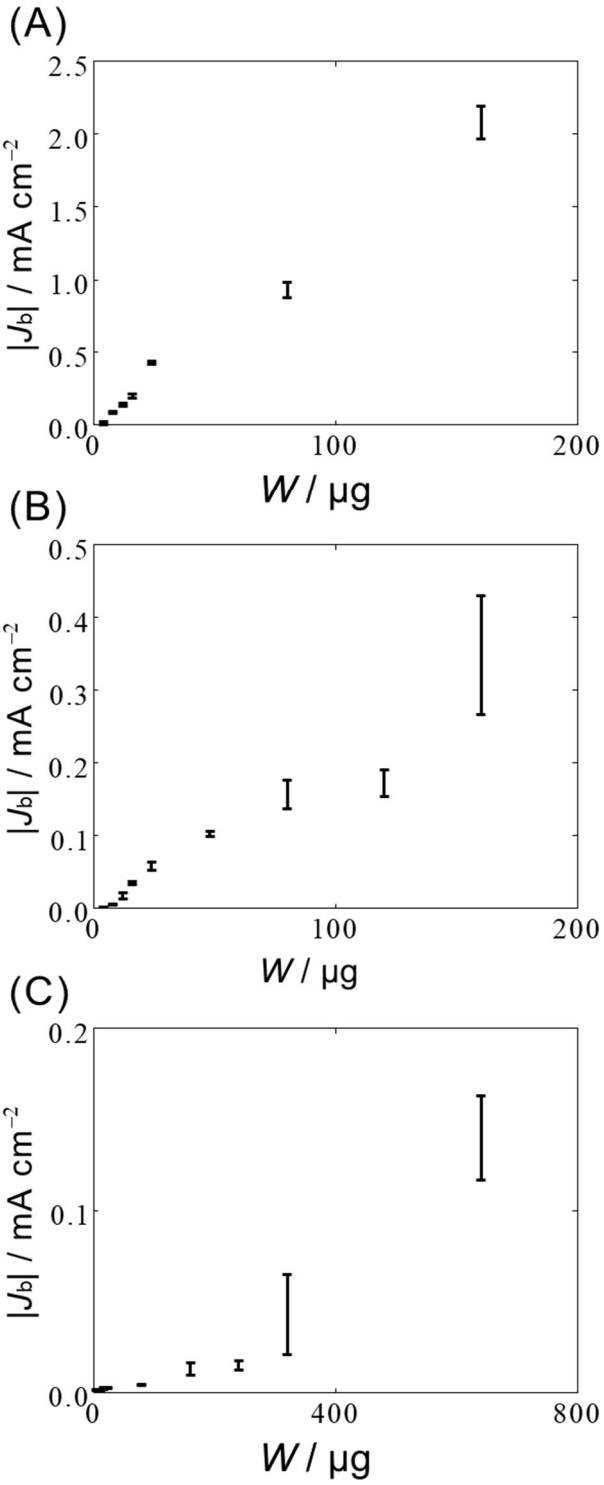

Fig. 2.9. Relationships between the charging current density and the weight of applied carbon materials; (A) KB, (B) Vulcan, and (C) JSP. The error bars indicate the confidence interval of 90%.

2.4. Conclusions

KB, Vulcan, and JSP have been investigated by electrochemically and microscopically as scaffolds for the DET-type bioelectrocatalysis of BOD in view of pore size, distribution of porous structures, and three-dimensional structures of the aggregated carbon materials. The comparison between KB and Vulcan shows that gap-type mesopores constructed three-dimensionally by the aggregation of KB or Vulcan particles with almost the same ϕ_p are effective as scaffolds for BOD thanks to curvature effects of the mesopores. Inside faces of partially broken KB particles are electrochemically active to give large $|j_b|$. However, the inner holes of KB are not effective as BOD scaffolds, since it is difficult for BOD to penetrate the hole. On the other hand, the surface structure of JSP is suitable for the DET-type bioelectrocatalysis of BOD most probably due to well-developed microstructures, on which fast electron transfer would proceeds. However, densely packed JSP was not suitable for the DET-reaction of BOD, most probably due to the hinderance in the penetration of BOD as well as mass-transfer of O_2.

The optimization of carbon material-modified electrodes for the DET-type bioelectrocatalysis requires to balance the ratio of macro-, meso, and micropores to construct the three-dimensional structure effective for the mass transport of electrolyte solution and substrates, as well as the penetration of enzymes into the nano-structures, and to enhance the interfacial electron transfer kinetics of macromolecular redox enzymes. The discussion based on the electrochemically active surface area as proposed in this work is important in the optimization of carbon materials for DET-type bioelectrocatalysis of redox enzymes.

References

1. I. Mazurenko, A. de Poulpiquet, and E. Lojou, *Curr. Opin. Electrochem.*, **5**, 1, (2017).
2. A. De Poulpiquet, A. Ciaccafava, and E. Lojou, *Electrochim. Acta*, **126**, 104, (2014).
3. T. Tamaki, *Top. Catal*. **55**, 1162, (2012)
4. A. Walcarius, S.D. Minteer, J. Wang, Y. Lin, and A. Merkoçi, *J. Mater. Chem*., **B1,** 4878, (2013).
5. D. Wen and A. Eychmüller, *Enzymatic biofuel cells on porous nanostructures, Small*, **12**, 4649, (2016).
6. R.A. Marcus, *Angew. Chem. Int. Ed*., **32**, 1111, (1993).
7. R.A. Marcus and N. Sutin, *BBA Rev. Bioenerg.*, **811**, 265, (1985).
8. I. Mazurenko, X. Wang, A. de Poulpiquet, and E. Lojou, *Sustain. Energy Fuels*, **1**, 1475, (2017).
9. D. Leech, P. Kavanagh, and W. Schuhmann, *Electrochim. Acta*, **84**, 223, (2012).
10. J.A. Cracknell, K.A. Vincent, and F.A. Armstrong, *Chem. Rev.*, **108**, 2439, (2008).
11. J. Wang, *Chem. Rev.*, **108**, 814, (2008).
12. D. Dollimore and G. R. Heal, *J. Appl. Chem.*, **14**, 109, (1964).
13. Y. Sugimoto, Y. Kitazumi, O. Shirai, and K. Kano, *Electrochemistry*, **85**, 82, (2017).
14. L. Bayne, R. V. Ulijn, and P.J. Halling, *Chem. Soc. Rev.*, **42**, 9000, (2013).
15. H. Funabashi, S. Takeuchi, and S. Tsujimura, *Sci. Rep.*, **7**, 1, (2017).
16. S. Hudson, J. Cooney, and E. Magner, *Angew. Chem. Int. Ed.*, **47**, 8582, (2008).
17. C.E. Zhao, P. Gai, R. Song, Y. Chen, J. Zhang, and J.J. Zhu, *Chem. Soc. Rev.*, **46**,

1545, (2017).

18. N. Mano, *Curr. Opin. Electrochem.*, **19**, 8, (2020).
19. J. Bhattarai, D. Neupane, B. Nepal, V. Mikhaylov, A. Demchenko, and K. Stine, *Nanomaterials*, **8**, 171, (2018).
20. M. Kizling, M. Dzwonek, A. Wieckowska, and R. Bilewicz, *Curr. Opin. Electrochem.*, **12**, 1, (2018).
21. K. Monsalve, M. Roger, C. Gutierrez-Sanchez, M. Ilbert, S. Nitsche, D. Byrne-Kodjabachian, V. Marchi, and E. Lojou, *Bioelectrochemistry*, **106**, 47, (2015).
22. U. Salaj-Kosla, S. Pöller, Y. Beyl, M.D. Scanlon, S. Beloshapkin, S. Shleev, W. Schuhmann, and E. Magner, *Electrochem. Commun.*, **16**, 92, (2012).
23. H. Qiu, C. Xu, X. Huang, Y. Ding, Y. Qu, and P. Gao, *J. Phys. Chem. C.*, **112**, 14781, (2008).
24. L. Lu, Y. Dong, J. Wang, Q. Li, and X. Wu, *Anal. Methods.*, **7**, 6686, (2015).
25. K. Nishio and H. Masuda, *Bull. Chem. Soc. Jpn.*, **86**, 1144, (2013).
26. Y. Deng, W. Huang, X. Chen, and Z. Li, *Electrochem. Commun.*, **10**, 810, (2008).
27. K. Sakai, Y. Kitazumi, O. Shirai, and K. Kano, *Anal. Sci.*, **34**, 1317, (2018).
28. Y. Mie, M. Ikegami, and Y. Komatsu, *Chem. Lett.*, **45**, 640, (2016).
29. C Léger and P Bertrand, *Chem. Rev.*, **108**, 2379, (2008).
30. Y. Miura, S. Tsujimura, S. Kurose, K.Kataoka, T. Sakurai, and K. Kano, *Fuel cells*, **9**, 70, (2009).
31. A. J. Bard and L R. Fraulkner, *Electrochemical methods: fundamentals and applications 2nd ed.*, Wiley, New York 335
32. S. Tsujimura, A. Nishina, Y. Hamano, K. Kano, and S. Shiraishi, *Electrochem. Commun.*, **12**, 446, (2010).

33. S. Maeno, *TANSO*, **2006,** 140, (2006).

34. S. Tsujimura, A. Nishina, Y. Kamitaka, and K. Kano, *Anal. Chem.*, **81**, 9383, (2009).

35. T. Adachi, Yuki Kitazumi, Osamu Shirai, and Kenji Kano, *Catalysis*, **10 (2)**, 236 (2020).

36. Y. Kitazumi, O. Shirai, M. Yamamoto, and K. Kano, *Electrochim. Acta*, **112**, 171, (2013).

37. Y. Takahashi, M. Wanibuchi, Y. Kitazumi, O. Shirai, and K. Kano, *J.Electroanaltical Chem.*, **843**, 47, (2019).

38. T. Siepenkoetter, U. Salaj-Kosla, X. Xiao, S. Belochapkine, and E. Magner, *Electroanalysis*, **28**, 2415, (2016).

Chapter 3

Enhancement of the Direct Electron Transfer-Type Bioelectrocatalysis of Bilirubin Oxidase at the Interface between Carbon Particles

The simulation model of the direct electron transfer (DET)-type bioelectrocatalysis at a porous electrode indicates that the catalytic current is proportional to the real surface area (A), when A is small. When A is large, the catalytic current is saturated at a limited value controlled by the mass transfer in the porous structure. In this study, the bioelectrocatalytic currents at porous electrodes are analyzed based on their charging currents. Comparisons among the carbon composites constructed with Vulcan and exfoliated graphite (JSP) show that the interface between the Vulcan and JSP particles is more suitable for the DET-type bioelectrocatalysis of bilirubin oxidase (BOD) than that between the particles of the same type. In particular, the most suitable properties were achieved at a Vulcan:JSP ratio of 1:1 in the composite electrode. In these composites, the multipoint contact between the BOD molecule and electrode seems to result in a higher DET-type bioelectrocatalytic activity.

3.1. Introduction

A bioelectrocatalytic reaction is the coupled reaction of the redox enzymatic reaction and the electrode reaction. When there is direct electron transfer between the enzyme and electrode, the coupled reaction is referred to as a direct electron transfer (DET)-type bioelectrocatalytic reaction[1–3]. Bilirubin oxidase (BOD) is one of the multicopper oxidases that can be used for the four-electron reduction of oxygen to water through DET-type bioelectrocatalysis[4]. BOD is widely employed as a biocathode catalyst in biofuel cells[5,6] because of its relatively high activity and relatively positive potential[7] in DET-type bioelectrocatalysis.

The electron transfer between the active redox center in the enzyme and the electrode is due to the tunneling effect[8–15]. Therefore, the distance of the electron transfer pathway and the orientation of the adsorbed enzyme at the electrode surface are considerably important in DET-type bioelectrocatalysis. BOD has two redox centers, a type 1 copper (T1) site and a type 2-3 copper (T2/3) cluster, in its structure[16–18]. The T1 site is regarded as the electrode active redox center of BOD[19]. The surface of BOD in the vicinity of the T1 site is positively charged for the BOD derived from *Myrothecium verrucaria*[20,21]. Therefore, the modification of the electrode surface with negatively charged aromatic compounds effectively improves the DET-type bioelectrocatalysis of BOD from *Myrothecium verrucaria*[10,20,22–27]. The different orientations of the adsorbed enzyme cause a distribution of the distance between the redox center and electrode. The distribution of the distance distorts the shape of the voltammogram of the DET-type bioelectrocatalytic process[9,28].

Porous electrodes are effective scaffolds for DET-type bioelectrocatalysis[29–31]. Previously, the DET-type bioelectrocatalysis of BOD has been improved on porous

carbons[31], porous metals[32], accumulated metal nanoparticles[32,33], carbon nanotubes[34,35], and accumulated graphene-modified electrodes[36,37]. According to the modeling of the DET-type bioelectrocatalysis of a spherical enzyme in a pore[9,32], the nanometer-sized pores at the electrode surface are important for the reaction. In the nanometer-sized pores, the enzyme makes multiple contacts with the electrode surface. The multiple contacts improve the probability of the enzyme has the effective orientation. Therefore, an electrode with nanometric pores on its surface is more advantageous than a planar electrode for the DET-type bioelectrocatalysis with an enzyme. The improvement in the DET-type bioelectrocatalysis on a porous structure has been explained by the curvature effect at the electrode surface[9].

The optimization of the enzyme orientation and the porous nanostructure at the electrode surface is important to improve the performance of the bioelectrode. However, it is difficult to separate the contributions of the surface property and the curvature effect at the electrode surface. In particular, analytical approaches for evaluating the DET-type bioelectrocatalysis at porous electrodes have been limited because the porous structure can affect the mass transfer of the substrate. As heterogeneous porous structures present many difficulties in determining the real surface area and identifying the surface composition, the comparisons among the electrode materials are frequently carried out on the basis of the amount of the porous material[38,39] rather than on the electrochemically effective surface area.

The determination of the electrochemically active surface area of a porous electrode is challenging[40]. The non-Faradaic current, which is proportional to the electrochemically active surface area, seems to be the most convenient parameter for evaluating it. Although it is assumed that the double layer capacities of the electrodes are

equal, the charging current is considered to be a good indicator of the electrochemically active surface area of a porous electrode. In the author's previous work[41], the DET-type bioelectrocatalytic reactions of BOD at the surface of various carbon particles, such as Ketjen Black (KB), Vulcan, and high-purity exfoliated graphite (JSP), were compared on the basis of the charging current. Moreover, the study showed that the interparticle interfaces between the primary particles of KB and Vulcan (KB/KB and Vulcan/Vulcan) are effective for the DET-type bioelectrocatalysis with BOD. Additionally, it was found that the hollow interior of the KB particle is not useful for DET-type bioelectrocatalysis. On the other hand, JSP, which is the largest particle among the studied carbon particles, had the most suitable surface for the DET-type bioelectrocatalysis of BOD.

In this study, the effect of the porous structure of the electrode on the mass transfer in the DET-type bioelectrocatalytic reaction is simulated by the finite element method. To investigate the interface between the carbon particles, composite electrodes were constructed using Vulcan and JSP, and the surfaces of the composite electrodes were visualized by scanning electron microscopy. The DET-type bioelectrocatalytic currents of BOD in these composites are compared on the basis of the charging currents. Finally, the orientations of BOD at these composites are discussed according to the random orientation model.

3.2. Model

Porous electrodes constructed with hexagonally close-packed spheres were considered for modeling. The spheres were assumed to be conductors, and the contact resistance was ignored. The space between the spheres was filled with an electrolyte solution. The substrate was able to diffuse freely in the electrolyte solution. According to the sizes of the carbon particles used in experimental studies[41], the diameter of the sphere (d_0) was set to 40 nm or 10 μm. The thicknesses of the porous layer and diffusion layer in the solution phase are denoted as l_p and l_d, respectively. The geometry of the model is shown in Fig. 3.1A. The DET-type bioelectrocatalytic reaction occurs at the surface of the spheres. To express the substrate consumption, the enzymatic reaction rate per unit area was calculated using the Michaelis–Menten equation:

$$v = \frac{k_C \Gamma_r c_s}{K_M + c_s}, \tag{3.1}$$

where c_S is the substrate concentration, K_M is the Michaelis constant, k_c is the catalytic constant, and Γ_r is the adsorbed amount of the enzyme per unit area of the real surface. Assuming the limiting current conditions, the kinetics of the electrode reactions were ignored in this model. The bulk concentration of the substrate outside the diffusion layer was kept constant at c_{s0}.

The real surface area of the electrode (A) was calculated as the summation of the surface areas of the spheres. The ratio of the real surface area to the projective surface area (A/A_0) is employed as the index of the porosity of the electrode. In this model, A/A_0 of 3.63 corresponds to a monolayer of close-packed spheres. The steady-state solution of the model was obtained using a commercially available finite element method package (COMSOL Multiphysics 5.5, COMSOL, Inc., USA). The steady-state current (j_{ss}) of the system was calculated by the following integration for the cross-section of the system (s):

$$j_{ss} = -\int_s n_S F D_S \frac{dc_S}{dx} ds\,, \tag{3.2}$$

where n_S, F, and D_S are the electron number of the substrate, Faraday constant, and diffusion coefficient of the substrate, respectively.

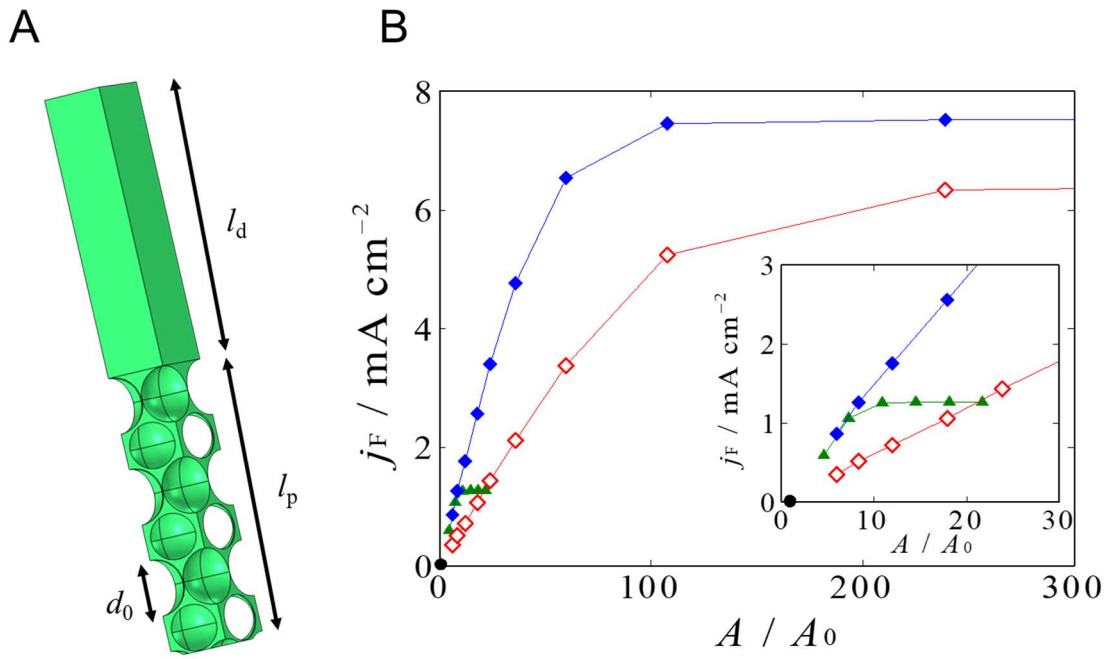

Fig. 3.1 (A) Geometry of the simulation model of the porous electrode. (B) Effect of the surface area on the simulated steady-state catalytic current when d_0 = 40 nm (diamonds) and 10 μm (triangles), v_{max} = 2×10^{-6} mol s^{-1} m^{-2} (open symbols) and 5×10^{-6} mol s^{-1} m^{-2} (filled symbols), and l_d = 10 μm. The inset in panel B shows the magnified view of the plot around the origin. The filled circle indicates the data point for a planar electrode without the bioelectrocatalytic activity.

3.3. Experimental section

3.3.1. Materials

BOD (EC 1.3.3.5) from *Myrothecium verrucaria* was purchased from Amano Enzyme Inc. (Japan), and used without further purification. Carbon materials such as Vulcan (primary particle size: 30–40 nm, Brunauer-Emmett-Teller (BET) surface area: 230 m^2 g^{-1}) and JSP (primary particle size: 10 μm, BET surface area: 11 m^2 g^{-1}) were purchased from Cabot Corporation (USA.) and Nippon Graphite Co., Ltd. (Japan), respectively[41]. Poly(1,1,2,2-tetrafluoroethylene) fine powder 6-J (PTFE) was purchased from DuPont-Mitsui Fluorochemicals Co., Ltd. (Japan). Unless otherwise specified, all other chemicals were of analytical grade and purchased from Wako Pure Chemical Industries, Ltd. (Japan). All solutions were prepared with ion-exchanged water.

3.3.2. Electrode preparation

Glassy carbon (GC) electrodes with a diameter of 3.0 mm (BAS, Japan) were polished with 0.05 μm alumina slurry and then cleaned by sonication and washing with ion-exchanged water. Each carbon material (40 mg) was mixed with PTFE (10 mg) as a binder and 3.5 mL (L = dm^3) of 2-propanol, and the mixture was homogenized with an ultrasonic homogenizer for 10 min. Thereafter, 6.5 mL of ion-exchanged water was added to the slurry, and the mixture was homogenized for 5 min with an ultrasonic homogenizer.

An appropriate amount of the carbon material mixture was cast on the surface of the polished GC electrode and dried at room temperature to evaporate the solvent. In the preparation of the carbon composite electrode, the homogenized slurries of JSP and Vulcan were mixed at the volume ratios of 1:9, 5:5, and 9:1 and homogenized for 1 min with sonication before casting. The corresponding composites are referred to as 1J9V,

5J5V, and 9J1V, respectively.

BOD (0.05 g) was dissolved in 250 μL of a 0.1 M (M = mol dm^{-3}) phosphate buffer (pH 7.0), and 10 μL of this BOD solution was spread on the carbon-material-modified GC electrodes. The electrodes were then allowed to stand in a water-saturated atmosphere for 1 h at 4 °C. The enzyme-adsorbed carbon-material-modified electrodes were washed with a phosphate buffer solution (pH 7.0) before electrochemical measurements.

3.3.3. Electrochemical measurements

All electrochemical measurements were conducted using an electrochemical analyzer (CompactStat, Ivium Technologies, Netherlands). Steady-state voltammetric measurements were carried out with rotating disk electrodes (RDEs) (RDE-1, BAS, Japan) at a rotating speed (ω) of 4000 rpm and scan rate (v) of 10 mV s^{-1} in an O_2-saturated 0.1 M phosphate buffer solution (pH 7.0). A platinum wire and Ag|AgCl|sat. KCl electrodes were used as the counter and reference electrodes, respectively. All potentials in this work are reported with respect to the reference electrode.

3.3.4. Scanning electron microscopy (SEM)

The surfaces of the carbon-material-modified electrodes were observed with a field emission scanning electron microscope (TM4000, Hitachi High-Technologies Co., Japan) at an acceleration voltage of 15.0 kV.

3.4. Results and discussion

3.4.1 Mass transfer and Faradaic processes at porous electrodes

Figure 3.1B shows the bioelectrocatalytic current at the porous electrode when l_d = 10 μm and K_M = 0.2 mM[23]. In this study, the current density (j) is defined as the current per projective unit area of the electrode. According to the Levich equation for oxygen in an aqueous solution (bulk concentration (c_{s0}) of 1.2 mM[42], electron number (n) of four, diffusion coefficient (D) of 2.1×10^{-9} m^2 s^{-1}, and kinematic viscosity (v) of 8.9×10^{-6} m^2 s^{-1} [42]), the value of l_d corresponds to that of the electrode at a rotating speed of 4000 rpm. The filled triangles and filled diamonds in Fig 3.1B show the results for the JSP model (d_0 = 10 μm) and the Vulcan model (d_0 = 40 nm) with $k_C\Gamma_r = 5\times10^{-6}$ mol s^{-1} m^{-2}, respectively. The increment in the surface area (that is, the widening of the porous layer) increased linearly with the steady-state current. Additionally, the steady-state currents in the low A/A_0 region were independent of the size of the particles. The open diamonds in Fig 3.1B indicate the steady-state current for the Vulcan model calculated at $k_C\Gamma_r = 2\times10^{-6}$ mol s^{-1} m^{-2}. The slope of this region is expressed by $nFk_c\Gamma_r$. Therefore, it is important to compare the bioelectrocatalytic activities of enzymes adsorbed at different porous electrodes according to the real surface area of the porous electrode[41].

On the other hand, the maximum values of the steady-state currents are 7.5 and 1.2 mA cm^{-2}, respectively, for the Vulcan and JSP model at $k_C\Gamma_r = 5\times10^{-6}$ mol s^{-1} m^{-2}. The difference in the maximum current suggests that the maximum value of the current is limited by the diffusion of species in the pores. Unfortunately, the maximum currents also depend on the value of $k_C\Gamma_r$ (shown in Supporting information (data not shown)). It is not possible to compare the surface properties based on the maximum current because the value is strongly affected by the porous structure. A comparison of the porous

electrode is possible only when the porosity of the electrode is sufficiently low. The simulation shows that the increase in the surface area per unit volume of the porous electrode is important for amplifying the substrate-transfer-limiting current.

3.4.2. Orientation of BOD at various carbon composites

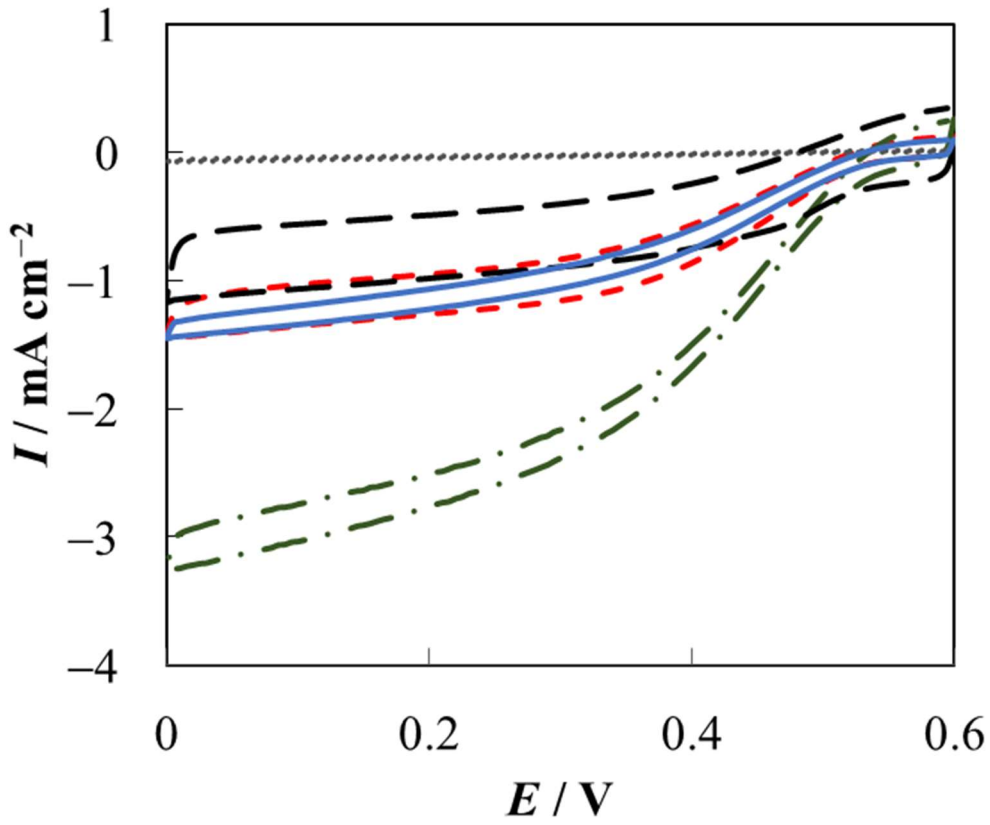

Fig. 3.2 Oxygen reduction RDCVs recorded with BOD adsorbed on electrodes modified with (dot-broken line) 160 μg Vulcan, (short dashed line) 640 μg JSP, (long dashed line)160 μg 1J9V, (solid line) 160 μg 5J5V, and (dotted line) 160 μg 9J1V. The data for JSP and Vulcan were reproduced from ref. 41 with permission from The Electrochemical Society of Japan.

Figure 3.2 shows the rotating-disk cyclic voltammograms (RDCVs) of the O_2 reduction through the DET-type bioelectrocatalysis of BOD adsorbed on electrodes modified with a large amount of various carbon components, (solid lines) 5J5V, (long-dashed lines) 1J9V, (short dashed lines) JSP, (dot-broken lines) Vulcan, and (dotted line) 9J1V. Clear sigmoidal voltammograms were obtained except for the case of 9J1V. The voltammograms suggest that BOD worked well as a DET-type bioelectrocatalyst in the four-electron reduction of O_2 at the surface of the carbon materials.

When a large amount of the carbon material was present at the electrode surface, the largest current was recorded with the Vulcan-modified electrode. The maximum value is approximately -3.5 mA cm^{-2}. On the other hand, the catalytic currents for the electrodes containing JSP were limited to approximately -1.5 mA cm^{-2}. According to the simulation model, the catalytic current at the porous electrode will be limited by the mass transfer of the substrate. Therefore, the large particles of JSP in the carbon composites will limit the mass transfer of the substrate in the porous carbon materials. Additionally, the substrate-transfer-limited current is insensitive to the ratio of JSP and Vulcan in the carbon composites. The catalytic and charging currents for the 9J1V modified electrode are quite small. Since the charging current is independent in the casted amount of 9J1V at the electrode surface, the number of conductive paths in this composite is quite small.

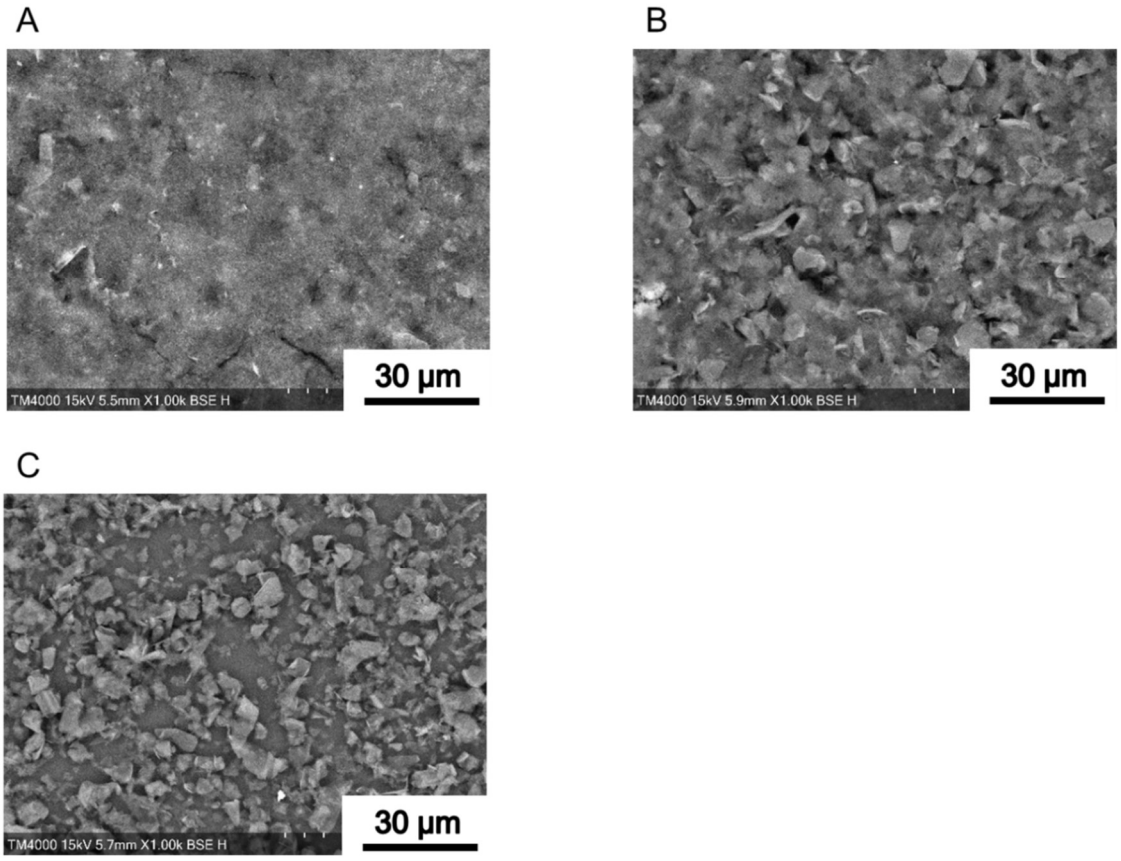

Fig. 3.3 SEM images of carbon composites with different volume ratios of JSP and Vulcan: (A) 1J9V, (B) 5J5V, and (C) 9J1V.

Figure 3.3 shows the SEM image of the surface of each carbon composite. At the resolution of the images, the primary particles of Vulcan are not identified. The surface of the 1J9V layer is mainly covered with Vulcan. In the case of 5J5V, the primary particles of JSP coated with Vulcan are separated from each other. On the other hand, in the case of 9J1V, the bare surface of JSP is exposed. Therefore, there is no attractive interaction between JSP particles and Vulcan particles.

To investigate the effect of the composite surface on the DET-type bioelectrocatalysis of BOD, the orientation of the adsorbed BOD was analyzed based on

the random orientation model[20]. When small amounts of the carbon materials are present at the electrode surface, the bioelectrocatalytic current is predominantly limited by the enzymatic reaction of BOD. Figure 3.4 shows the RDCVs for small amounts of carbon composites with a maximum current of approximately −0.3 mA cm^{-2}. Because the bioelectrocatalytic currents are smaller than the substrate-limited value, the currents are mainly controlled by the enzymatic reaction. In these voltammograms, the onset potential of the bioelectrocatalytic oxygen reduction appeared at 0.5 V. These voltammograms do not have a clear sigmoidal shape. The bioelectrocatalytic oxygen reduction current depended linearly on the applied potential in the potential region more negative than 0.4 V. The slope of the voltammograms is referred to as the residual slope[8,15,20]. The existence of the residual slope on the voltammogram indicates the randomly oriented enzyme molecules at the electrode surface.

Although the catalytic currents were lower than the diffusion-limited currents, the contribution of mass transfer to the catalytic current was still large. To eliminate the effect of mass transfer on the catalytic current, a serially connected resistances model is considered here. Considering bioelectrocatalysis at the porous RDE, the j value can be given by the following Koutecký-Levich-type equation combined with the mass transfer in the porous structure:

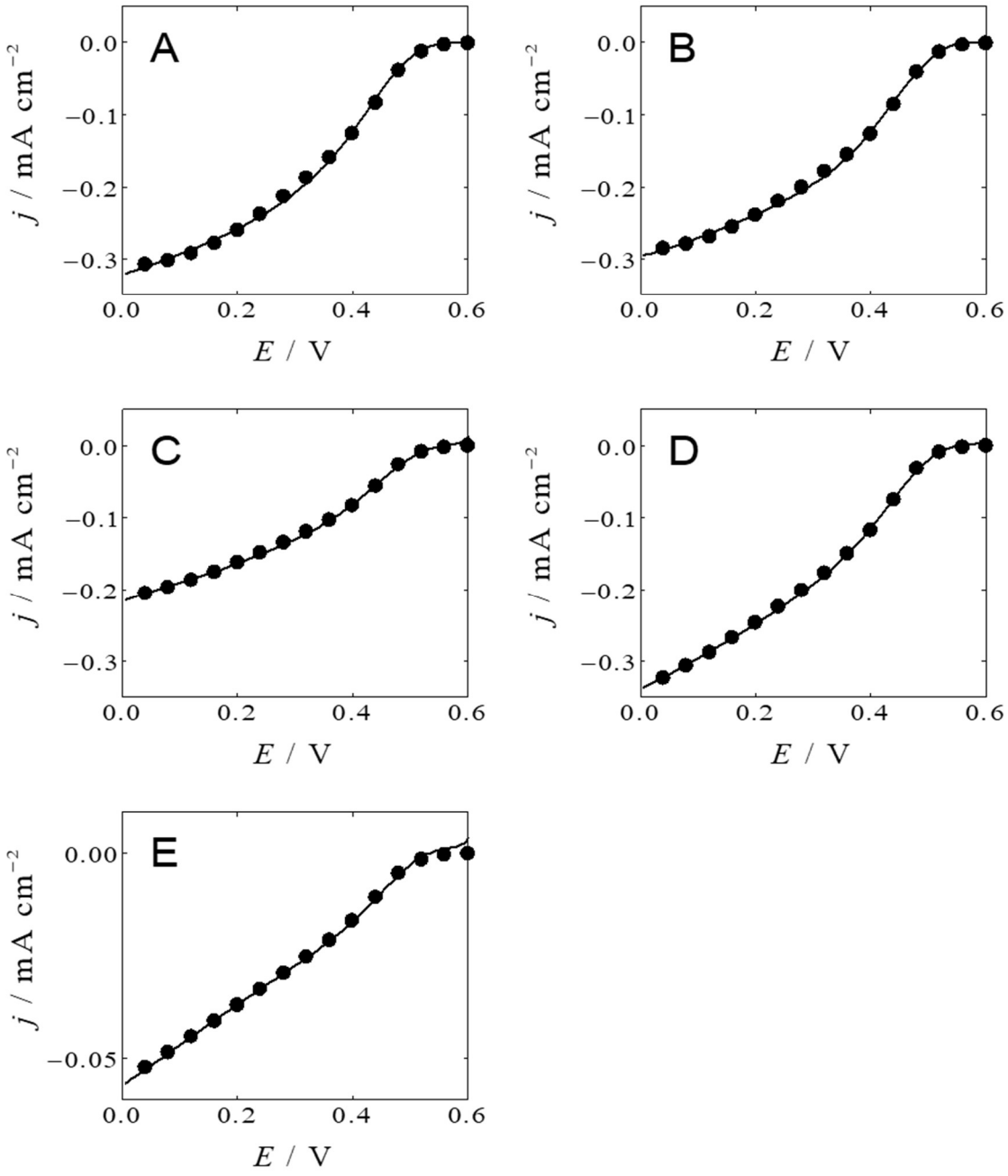

Fig. 3.4 Oxygen reduction RDCVs recorded with BOD adsorbed on electrodes modified with (A) 8 μg Vulcan, (B) 80 μg JSP, (C) 16 μg 1J9V, (D) 8 μg 5J5V, and (E) 16 μg 9J1V. The circles represent the best fit of the data to Eq. 3.3.

$$\frac{1}{j} = \frac{1}{j_{\mathrm{d}}} + \frac{1}{j_{\mathrm{c}}} + \frac{1}{j_{\mathrm{p}}} \tag{3.3}$$

where j_{d}, j_{c}, and j_{p} are, respectively, the limiting current densities controlled by the mass transfer of O_2 in the bulk solution at the RDE, the enzymatic reaction kinetics, and the mass transfer in the porous structure. In the case of the four-electron reduction of oxygen, the j_{d} value in an O_2-saturated aqueous solution can be estimated by the Levich equation to be 8.4 mA cm^{-2} at ω = 4000 rpm and 25 °C. The value of j_{c} is given by the random orientation model[20], as follows:

$$j_{\mathrm{c}} = \frac{j_{\mathrm{c,max}}}{\beta \Delta d (1 + \exp\{\Phi\})} \ln \left| \frac{\frac{k_0^{\max}}{k_{\mathrm{c}}}(1 + \exp\{\Phi\}) + \exp\{\alpha\Phi\}}{\frac{k_0^{\max}}{k_{\mathrm{c}}}\exp(-\beta\Delta d)(1 + \exp\{\Phi\}) + \exp\{\alpha\Phi\}} \right|, \tag{3.4}$$

where

$$\Phi = \frac{n_{\mathrm{E}} F}{RT}(E - E^{\circ\prime}{}_{\mathrm{E}}), \tag{3.5}$$

$$j_{\mathrm{c,max}} = -n_{\mathrm{E}} F k_{\mathrm{c}} \Gamma, \tag{3.6}$$

β is the coefficient of the long-range electron transfer, Δd is the difference in the distance between the closest and farthest approaches of the redox center of an enzyme that electrochemically communicates with an electrode, n_{E} is the number of electrons in the rate-determining step of the interfacial electron transfer (= 1 for the T1 site in BOD), R is the gas constant, T is the absolute temperature, $E^{\circ\prime}{}_{\mathrm{E}}$ is the formal potential of the redox center of the enzyme, $k_0^{\max}$ is the standard rate constant at the distance of the closest approach in the best orientation of the enzyme, k_{c} is the DET-type catalytic constant of the enzyme, and α is the transfer coefficient.

As mentioned above, the theoretical estimation of the value of j_{P} is difficult. In this work, the value of $1/(1/j_{\mathrm{d}} + 1/j_{\mathrm{p}})$ was estimated from the experimentally recorded maximum current when a sufficient amount of the carbon material was present at the

electrode surface (−3.5 mA cm^{-2} for Vulcan and −1.5 mA cm^{-2} for JSP-containing composites). Using $j_{c,max}$, $\beta\Delta d$, k_0^{max}/k_c, and α as adjustable parameters, Eq. 3.3 was fitted to the voltammograms using non-linear regression analysis with Gnuplot. In this fitting, the employed value of $E°'_E$ is 0.46 V[43]. The parameters corresponding to the best fits to the voltammograms shown in Fig. 3.4 are listed in Table 3.1.

Table 3.1 Best-fitted parameters to the experimentally recorded voltammograms.

	Vulcan	**JSP**	**1J9V**	**5J5V**	**9J1V**
$j_{c,max}$ / mA cm^{-2}	−0.359±0.002	−0.381±0.002	−0.263±0.003	−0.476±0.005	0±70
$\beta\Delta d$	9±1	10±1	11±1	16±2	0±10^4
$\frac{k_0^{max}}{k_c}$	10±4	17±6	18±6	24±8	30±6
α	0.50±0.05	0.51±0.05	0.50±0.04	0.76±0.07	0.56±0.07
j_b / mA cm^{-2}	0.0048	0.0046	0.0076	0.0018	0.0039
$\frac{\lvert j_{c,max}\rvert}{j_b}$	74.3±0.4	82.4±0.4	22.1±0.3	297±3	-
$\frac{k_0^{max}\lvert j_{c,max}\rvert}{k_c j_b}$	700±300	1400±500	400±100	7000±2000	-

The regression analysis for the 9J1V-modified electrode resulted in a large error because the potential-independent current limited by the enzymatic reaction was not observed in the voltammogram.

To compare the carbon materials, an appropriate normalization of the electrode surface area is required. According to the comparison of the BET surface area and charging current, there is no significant difference between the double layer capacitances of Vulcan and JSP (shown in Fig. 3.5). Here, the author employs the charging current as an indicator of the real surface area of the electrode surface. In this analysis, the charging current (j_b) was estimated from the voltammogram as the difference between the anodic and cathodic currents of RDCV at 0.55 V.

According to Eq. 3.4, the value of $j_{c,max}/j_b$ is proportional to $k_c \Gamma_r$. Vulcan and JSP have almost the same values of $j_{c,max}/j_b$. On the other hand, 5J5V has the largest value of $j_{c,max}/j_b$ among the inspected composites (Table 3.1). This result shows that an appropriate mixing ratio of Vulcan and JSP creates a more suitable scaffold for the bioelectrocatalysis of BOD.

When the surface of the carbon composite is saturated with BOD, the value of Γ_r is constant for each composite. Under this assumption, the value of $(k_0 j_{c,max})/(k_c j_b)$ is proportional to k_0. The estimated value for 5V5J is very large compared to those of other composites (Table 1). However, the results seem to be affected by the difference in the effective amount of BOD for each carbon composite. The surface structure constructed at 5J5V provides multipoint contact between BOD and the electrode. Therefore, the effective amount of BOD at 5J5V becomes larger than that at the other composites.

The value of $\beta\Delta d$ at 5J5V is significantly larger than the values at the other carbon composites. The multipoint contact enables that BOD receives electrons from the

electrode at various angles. Therefore, the multipoint contact at the electrode surface increases the value of $\beta\Delta d$. The expectation of multipoint contact of BOD at 5J5V surface is supported by the increase in the effective amount of BOD with the increase in $\beta\Delta d$.

3.4.3. Effect of the amount of carbon composites

The DET-type bioelectrocatalysis, fundamentally, depends on the electrochemically active surface area of the electrode. In this work, the background-subtracted current density recorded at 0 V was defined as the limiting current density ($j_{lim} = j - j_b$). Figure 3.5 shows the j_b value-dependence of j_{lim} for various carbon composites. The value of j_{lim} increased with j_b in the low j_b region and showed saturation behavior in the high j_b region at every carbon-material-modified electrode, except for 9J1V. These experimentally recorded trends agree with the relationship between A/A_0 and j_F shown in Fig. 3.1B from the model calculation. Additionally, the saturated values of j_{lim} in Fig. 3.5 agree with those in Fig. 3.2.

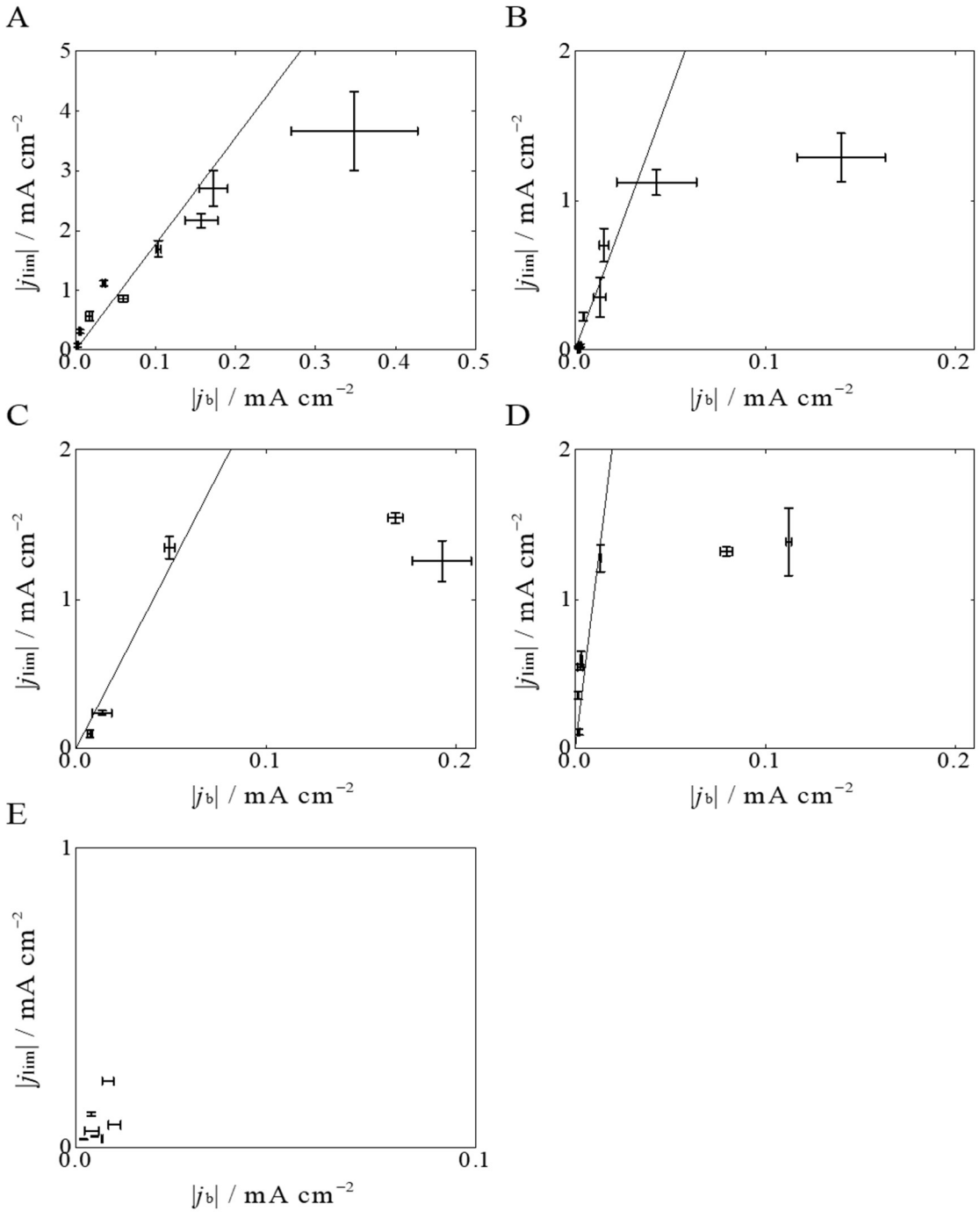

Fig. 3.5 Relationships between the absolute values of the bioelectrocatalytic current density and the background current density for (A) Vulcan, (B) JSP, (C) 1J9V, (D) 5J5V, and (E) 9J1V. Error bars indicate 90% confidence intervals for j_{lim} and j_b for each electrode.

Assuming that the value of j_{lim} is proportional to j_b in the low j_b region, the slopes of the linear regions are 18±1, 34±3, 24±1, and 104±9 for Vulcan, JSP, 1J9V, and 5J5V, respectively. According to the model calculation, this slope is proportional to $k_C\Gamma_r$. Moreover, the value of $j_{c,max}/j_b$ is also proportional to $k_C\Gamma_r$. Both the results shown in Table 3.1 and Fig. 3.4 indicate that the surface of 5J5V is the most effective scaffold for the DET-type bioelectrocatalysis of BOD. In the case of 1J9V, the expectation of the surface property from the slope in Fig. 3.4 C disagrees with that from $j_{c,max}/j_b$. This discrepancy is possibly due to the difference between the experimentally determined j_{lim} and j calculated with the model. The model calculation assumes the limiting current conditions for bioelectrocatalysis. However, the experimentally recorded current is still under the effect of the residual slope. Therefore, further analysis of the BOD orientation combined with the mass transfer limitation in the porous electrode is required.

3.4.4. Effects of the lamination of carbon materials

The above discussion is for homogenized carbon composites. The effect of the lamination of the carbon materials was investigated further. Figure 3.6 shows the bioelectrocatalytic current for the composite materials with (A) Vulcan overlaid on the JSP layer and (B) JSP overlaid on the Vulcan layer.

When the Vulcan layer is formed on the JSP layer, the value of j_{lim} increases with an increase in the casted amount of Vulcan. The saturated value of j_{lim} agrees with that of the Vulcan-modified electrode. When a large amount of Vulcan is added, the JSP particles are buried within Vulcan. Therefore, the composite seems to work like a Vulcan electrode when a sufficient amount of Vulcan was cast on the JSP layer.

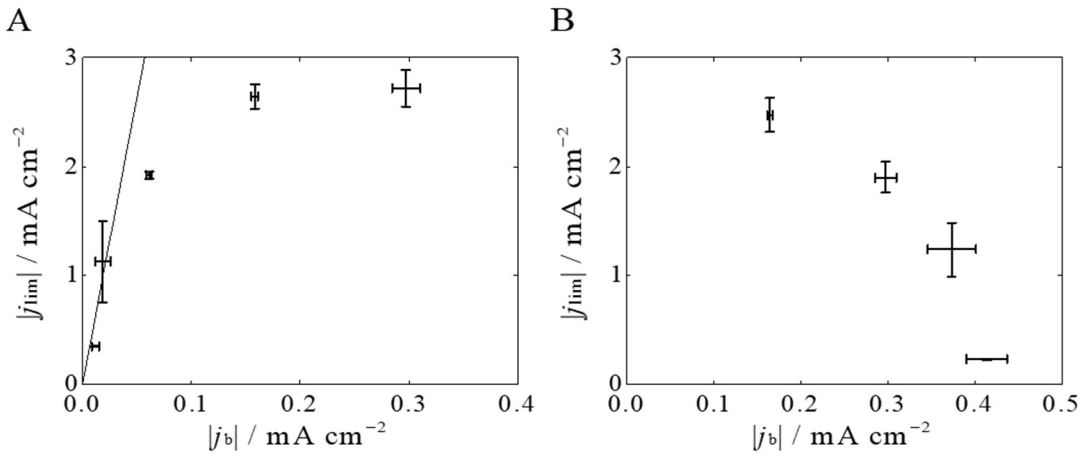

Fig. 3.6 Relationships between the absolute values of the bioelectrocatalytic current density and the background current density for (A) different amounts of Vulcan overlaid on the JSP layer (80 μg) and (B) various amounts of JSP overlaid on the Vulcan layer (80 μg).

Interestingly, the increment in j_{lim} in the low j_b region is steeper. The estimated slope in the low j_b region is 52±4, which is larger than that for Vulcan or JSP. Therefore, Vulcan casted on the JSP layer can be inferred to have led to Vulcan-coated JSP particles, as in the case of 5J5V, at the electrode surface. An increase in the casted amount of JSP in the Vulcan layer leads to a decrease in the value of j_{lim}. The decreased value of j_{lim} is lower than the value of the saturated current recorded with the JSP-modified electrode. Therefore, the accumulated JSP layer not only induces resistance to substrate transfer to the Vulcan layer but also to the electrochemically inactive insulation layer. The insufficient electrical contacts of the upper part of the JSP layer indicate that there is hardly any electrical connection between the JSP particles.

3.5. Conclusions

A theoretical model was constructed for analyzing the porous electrode surface as the scaffold of the DET-type bioelectrocatalysis. The porous structure of the electrode affected the substrate transfer and limited the mass-transfer-controlled current. Based on the model, the surface properties of the carbon composites constructed with JSP and Vulcan were compared for the scaffold of the DET-type bioelectrocatalysis of BOD. The analysis suggests that the interface between the JSP and Vulcan particles is a more effective scaffold than the interface between the individual JSP particles or Vulcan particles. According to the orientational analysis of the adsorbed enzyme, there are many contact points between BOD and the electrode at the JSP/Vulcan interface than at the other interfaces (JSP/JSP or Vulcan/Vulcan).

References

1. J. E. Frew and H. A. O. Hill, *Eur. J. Biochem.*, **172**, 261 (1988).
2. A. L. Ghindilis, P. Atanasov, and E. Wilkins, *Electroanalysis*, **9**, 661 (1997).
3. Y. Kamitaka, S. Tsujimura, N. Setoyama, T. Kajino, and K. Kano, *Phys. Chem. Chem. Phys.*, **9**, 1793 (2007).
4. S. Tsujimura, T. Nakagawa, K. Kano, and I. Tokuji, *Electrochemistry*, **72**, 437 (2004).
5. I. Willner, Y.-M. Yan, B. Willner, and R. Tel-Vered, *Fuel Cells*, **9**, 7 (2009).
6. M. Rasmussen, S. Abdellaoui, and S. D. Minteer, *Biosens. Bioelectron.*, **76**, 91 (2016).
7. S. C. Barton, J. Gallaway, and P. Atanassov, *Chem. Rev.*, **104**, 4867 (2004).
8. C. Léger, A. K. Jones, S. P. J. Albracht, and F. A. Armstrong, *J. Phys. Chem. B*, **106**, 13058 (2002).
9. Y. Sugimoto, Y. Kitazumi, O. Shirai, and K. Kano, *Electrochemistry*, **85**, 82 (2017).
10. K. So, S. Kawai, Y. Hamano, Y. Kitazumi, O. Shirai, M. Hibi, J. Ogawa, and K. Kano, *Phys. Chem. Chem. Phys.*, **16**, 4823 (2014).
11. R. J. Lopez, S. Babanova, Y. Ulyanova, S. Singhal, and P. Atanassov, *ChemElectroChem*, **1**, 241 (2014).
12. N. Lalaoui, K. Elouarzaki, A. Le Goff, M. Holzinger, and S. Cosnier, *Chem. Commun.*, **49**, 9281 (2013).
13. A. A. Arrocha, U. Cano-Castillo, S. A. Aguila, and R. Vazquez-Duhalt, *Biosens. Bioelectron.*, **61**, 569 (2014).
14. A. dePoulpiquet, D. Ranava, K. Monsalve, M. T. Giudici-Orticoni, and E. Lojou, *ChemElectroChem*, **1**, 1724 (2014).

15. C. Léger and P. Bertrand, *Chem. Rev.*, **108**, 2379 (2008).

16. E. I. Solomon, U. M. Sundaram, and T. E. Machonkin, *Chem. Rev.*, **96**, 2563 (1996).

17. Y. Kamitaka, S. Tsujimura, K. Kataoka, T. Sakurai, T. Ikeda, and K. Kano, *J. Electroanal. Chem.*, **601**, 119 (2007).

18. T. Sakurai and K. Kataoka, *Chem. Rec.*, **7**, 220 (2007).

19. A. A. Gewirth and M. S. Thorum, *Inorg. Chem.*, **49**, 3557 (2010).

20. H. Q. Xia, Y. Kitazumi, O. Shirai, and K. Kano, *J. Electroanal. Chem.*, **763**, 104 (2016).

21. I. Mazurenko, K. Monsalve, J. Rouhana, P. Parent, C. Laffon, A. Le Goff, S. Szunerits, R. Boukherroub, M.-T. Giudici-Orticoni, N. Mano, and E. Lojou, *ACS Appl. Mater. Interfaces*, **8**, 23074 (2016).

22. M. Falk, V. Andoralov, Z. Blum, J. Sotres, D. B. Suyatin, T. Ruzgas, T. Arnebrant, and S. Shleev, *Biosens. Bioelectron.*, **37**, 38 (2012).

23. L. Dos Santos, V. Climent, C. F. Blanford, and F. A. Armstrong, *Phys. Chem. Chem. Phys*, **12**, 13962 (2010).

24. A. Kapp, M. K. Beissenhirtz, F. Geyer, F. Scheller, M. S. Viezzoli, and F. Lisdat, *Electroanalysis*, **18**, 1909 (2006).

25. G. Göbel and F. Lisdat, *Electrochem. Commun.*, **10**, 1691 (2008).

26. M. Tominaga, M. Ohtani, and I. Taniguchi, *Phys. Chem. Chem. Phys.*, **10**, 6928 (2008).

27. Y. Ogawa, S. Yoshino, T. Miyake, and M. Nishizawa, *Phys. Chem. Chem. Phys.*, **16**, 13059 (2014).

28. V. Fourmond and C. Léger, *Curr. Opin. Electrochem.*, **1**, 110 (2017).

29. S. D. Minteer, B. Y. Liaw, and M. J. Cooney, *Curr. Opin. Biotechnol.*, **18**, 228 (2007).

30. J. Kim, H. Jia, and P. Wang, *Biotechnol. Adv.*, **24**, 296 (2006).

31. V. Flexer, N. Brun, O. Courjean, R. Backov, and N. Mano, *Energy Environ. Sci.*, **4**, 2097 (2011).

32. Y. Takahashi, M. Wanibuchi, Y. Kitazumi, O. Shirai, and K. Kano, *J. Electroanal. Chem.*, **843**, 47 (2019).

33. V. Krikstolaityte, A. Barrantes, A. Ramanavicius, T. Arnebrant, S. Shleev, and T. Ruzgas, *Bioelectrochemistry*, **95**, 1 (2014).

34. O. Yehezkeli, R. Tel-vered, J. Wasserman, A. Trifonov, D. Michaeli, R. Nechushtai, and I. Willner, *Nat. Commun.*, **3**, 742 (2012).

35. K. So, M. Onizuka, T. Komukai, Y. Kitazumi, O. Shirai, and K. Kano, *Electrochim. Acta*, **192**, 133 (2016).

36. S. Shiba, J. Inoue, D. Kato, K. Yoshioka, and O. Niwa, *Electrochemistry*, **83**, 332 (2015).

37. J. Filip, A. Andicsová-Eckstein, A. Vikartovská, and J. Tkac, *Biosens. Bioelectron.*, **89**, 384 (2017).

38. K. So, H. Ozawa, M. Onizuka, T. Komukai, Y. Kitazumi, O. Shirai, and K. Kano, *Electrochim. Acta*, **246**, 794 (2017).

39. S. Tsujimura, M. Oyama, H. Funabashi, and S. Ishii, *Electrochim. Acta*, **322**, 134744 (2019).

40. C. Fisica and U. Milano, *Pure Appl. Chem.*, **63**, 711 (1991).

41. M. Wanibuchi, Y. Takahashi, Y. Kitazumi, O. Shirai, and K. Kano, *Electrochemistry*, **88**, 374 (2020).

42. W. Xing, M. Yin, Q. Lv, Y. Hu, C. Liu, and J. Zhang, "*Rotating Electrode Methods and Oxygen Reduction Electrocatalysts*", (Ed. W. Xing, G. Yin, and J. Zhang), Elsevier B.V., 1 , (2014).

43. S. Tsujimura, A. Kuriyama, N. Fujieda, K. Kano, and T. Ikeda, *Anal. Biochem.*, **337**, 325 (2005).

General Conclusion

In Chapter 1, porous Au electrodes have been prepared under several anodizing conditions, and the effects of the porous structures on the DET-type bioelectrocatalytic performance of BOD have been investigated. The mesoporous structure of the Au surface is convenient for DET-type bioelectrocatalysis of BOD, because the 3-D porous structure on the electrode surface enhances the curvature effects for the adsorbed BOD. The surface area of the porous Au electrode can be enlarged by increasing the anodization time to some extent, though saturation behavior was observed at increased anodization due to the limitations of O_2 transport from the bulk phase and the adsorption of BOD in deep layers. The DET-type bioelectrocatalytic activity of BOD is mainly determined by the surface area of the mesoporous Au electrodes and in part of the glucose concentration during anodization. The anodizing potential is not an important factor governing the DET-type activity. The SEM observations and the simple closed-packing sphere model has also supported the significance of the mesoporous structures in providing curvature effects for the DET-type reaction. The procedure described here may generate several mesoporous structures suitable for a variety of redox enzymes.

In Chapter 2, KB, Vulcan, and JSP have been investigated by electrochemical and microscopically as scaffolds for the DET-type bioelectrocatalysis of BOD in view of pore size, distribution of porous structures, and three-dimensional structures of the aggregated carbon materials. The comparison between KB and Vulcan shows that gap-type mesopores constructed three-dimensionally by the aggregation of KB or Vulcan particles with almost the same ϕ_p are effective as scaffolds for BOD thanks to curvature effects of the mesopores. Inside faces of partially broken KB particles are

electrochemically active to give large $|j_b|$. However, the inner holes of KB are not effective as BOD scaffolds, since it is difficult for BOD to penetrate the hole. On the other hand, the surface structure of JSP is suitable for the DET-type bioelectrocatalysis of BOD most probably due to well-developed microstructures, on which fast electron transfer would proceed. However, densely packed JSP was not suitable for the DET-reaction of BOD, most probably due to the hinderance in the penetration of BOD as well as mass-transfer of O_2.

The optimization of carbon material-modified electrodes for the DET-type bioelectrocatalysis requires to balance the ratio of macro-, meso, and micropores to construct the three-dimensional structure effective for the mass transport of electrolyte solution and substrates, as well as the penetration of enzymes into the nano-structures, and to enhance the interfacial electron transfer kinetics of macromolecular redox enzymes. The discussion based on the electrochemical active surface area as proposed in this work is important in the optimization of carbon materials for DET-type bioelectrocatalysis of redox enzymes.

In Chapter 3, a theoretical model was constructed for analyzing the porous electrode surface as the scaffold of the DET-type bioelectrocatalysis. The porous structure of the electrode affected the substrate transfer and limited the mass-transfer-controlled current. Based on the model, the surface properties of the carbon composites constructed with JSP and Vulcan were compared for the scaffold of the DET-type bioelectrocatalysis of BOD. The analysis suggests that the interface between the JSP and Vulcan particles is a more effective scaffold than the interface between the individual JSP particles or Vulcan particles. According to the orientation analysis of the adsorbed enzyme, there are many contact points between BOD and the electrode at the JSP/Vulcan interface than at the

other interfaces (JSP/JSP or Vulcan/Vulcan).

Acknowledgement

The author wishes to express her sincere gratitude to Dr. Osamu Shirai, Professor of Kyoto University for providing her with his constructive comments.

The author would like to thank Dr. Yuki Kitazumi, Assistant Professor of Kyoto University, for his kind supports and a number of comments.

The author is deeply appreciative of Professor Emeritus Kenji Kano for his strict opinions and advice, as well as for his encouragement and assistance.

The author wishes to express her heartfelt appreciation to Ms. Yui Takahashi, as a collaborator. The author would like to express her sincere gratitude to Dr. Masafumi Asahi for providing the equipment, research advice, and encouragements.

The author would like to thank Dr. Akira Yoshino of the Lithium-Ion Battery Technology Evaluation Center Consortium (LIBTEC) for allowing her to transfer to the doctoral program. And the author also appreciate the encouragement of her colleagues.

The author gratefully thanks to the members of Shirai's laboratory and Mrs.Toshie Koyama, for their kind support in the author's laboratory life.

The author thanks professors and doctors the author has ever met in conferences and events for their kind advices and encouragements.

Finally, the author would like to express her greatest thanks to her family and friends for their continuous encouragements.

Mizue Wanibuchi

Kyoto

March 2021

List of Publications

1) Yui Takahashi, Mizue Wanibuchi, Yuki Kitazumi, Osamu Shirai, Kenji Kano
Improved Direct Electron Transfer-type Bioelectrocatalysis of Bilirubin Oxidase using Porous Gold Electrodes
Journal of Electroanalytical Chemistry, **843**, 47-53 (2019). (Chapter 1)

2) Mizue Wanibuchi, Yui Takahashi, Yuki Kitazumi, Osamu Shirai, Kenji Kano
Significance of Nano-structures of Carbon Materials for Direct-electron-transfer-type Bioelectrocatalysis of Bilirubin Oxidase
Electrochemistry, **88**, 1-6 (2020). (Chapter 2)

3) Mizue Wanibuchi, Yuki Kitazumi, Osamu Shirai, Kenji Kano
Enhancement of the Direct Electron Transfer-type Bioelectrocatalysis of Bilirubin Oxidase at the Interface between Carbon Particles
Electrochemistry, *Electrochemistry*, **88**, 374–379 (2020). (Chapter 3)